SHEDDING LIGHT ON TIME SERIES CLASSIFICATION USING INTERPRETABILITY GATED NETWORKS

Anonymous authors
Paper under double-blind review

ABSTRACT

In time-series classification, interpretable models can bring additional insights but be outperformed by deep models since human-understandable features have limited expressivity and flexibility. In this work, we present InterpGN, a framework that integrates an interpretable model and a deep neural network. Within this framework, we introduce a novel gating function design based on the confidence of the interpretable expert, preserving interpretability for samples where interpretable features are significant while also identifying samples that require additional expertise. For the interpretable expert, we incorporate shapelets to effectively model shape-level features for time-series data. We introduce a variant of Shapelet Transforms to build logical predicates using shapelets. Our proposed model achieves comparable performance with state-of-the-art deep learning models while additionally providing interpretable classifiers for various benchmark datasets. We further show that our models improve on quantitative shapelet quality and interpretability metrics over existing shapelet-learning formulations. Finally, we demonstrate the capability of our models to provide interpretability in a real-world application using the MIMIC-III dataset.

1 INTRODUCTION

Time series classification is a fundamental task for time series (TS) data. Depending on the number of observed variables, TS classification problems can be categorized as either univariate or multivariate. Both categories are involved in a wide range of applications. Univariate TS data includes image outlines, sound, and spectrographs, and multivariate TS data include electroencephalogram (EEG), electrocardiogram (ECG), and human activity recognition (HAR). These types of TS data appear in essential applications such as healthcare, neuroscience, and automation. In recent years, there has been an increasing trend of employing deep learning models to TS classification problems. However, despite achieving state-of-the-art performance, deep models typically lack interpretability.

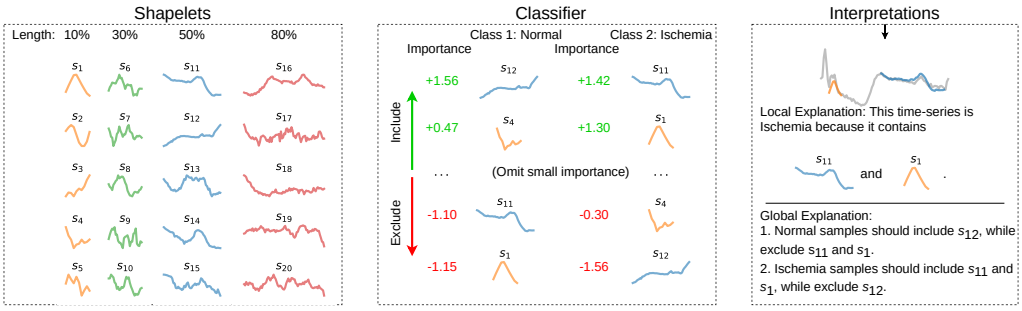

Figure 1: An example of shapelet-based interpretable TS classification on the *ECG200* dataset. (Left) The set of shapelets with various lengths to capture features with different scales. (Middle) A classifier that associates the shapelets with categories, assigning importance scores to them. (Right) Two methods to interpret the classifier result in rule-like explanations.

As a motivating example for interpretable TS classification, consider the problem of classifying ECG data using machine learning (Neves et al., 2021; Abdullah et al., 2023; Aziz et al., 2021). While models might be accurate, doctors may hesitate to rely on them without understanding why a patient's heartbeat as measured by an ECG was classified as being indicative of reduced bloodflow to the heart (known as myocardial ischemia). Our model seeks to provide such trust by discovering classifiers based on understandable concepts, such as those illustrated in Figure 1 (middle), where heartbeats are classified according to the existence of patterns known as shapelets. In this example, shapelet s_{11}, representing a downward trend, and s_{12}, representing an upward trend, serve as discriminative patterns that classify normal and ischemic heartbeats. A doctor may gain confidence in seeing such patterns with straightforward interpretations, such as in Figure 1 (right), that were deemed important to the predictions.

Interpretability can be significant from two perspectives. Firstly, in applications such as healthcare and physical systems where safety is essential, interpreting a model allows us to validate reliability, trustworthiness, and fairness. Secondly, in challenging tasks, we can gain knowledge about the problem by interpreting patterns found by machine learning models during training. Existing interpretable time series methods (Zhao et al., 2023) include *post hoc* explainability which explain the behavior of a trained deep learning model often using a surrogate model (Queen et al., 2023), and self-explainable models for which model predictions are directly interpretable.

In this study, we focus on self-explainable models. A recent self-explainable TS model, Neuro-Symbolic Time Series Classification (NSTSC) (Yan et al., 2022), combines a neuro-symbolic model (Riegel et al., 2020) with signal temporal logic (Mehdipour et al., 2021); soft-logic predicates are defined on each time stamp, and logic rules are learned to describe the classes. Although such approaches are defined to be interpretable, identifying the logical rules when applied to complex tasks can result in numerous predicates and logical operators. Furthermore, it is known that interpretability may lead to lower classification performance due to incomplete coverage of interpretable concepts or limited expressivity (Koh et al., 2020; Oikarinen et al., 2022; Havasi et al., 2022); such is the case for Concept Bottleneck Models (CBMs) (Koh et al., 2020), a popular interpretable model in computer vision. Similarly in TS, time-domain features (such as shapes and trends) are easy to understand but may not be able to capture other essential features such as those in the frequency domain.

In addition to post-hoc explanations, the literature on combining black-box models with interpretable models includes approaches such as performing logical reasoning on concepts discovered by deep models (Lee et al., 2022) or using deep models to select from a set of interpretable primitives, which are then composed to form the final predictions (Okajima & Sadamasa, 2019). In this paper, with the NEW
goal of maintaining interpretability when appropriate while allowing for additional complexity where concept-level information is not significant, we propose an Interpretability Gated Network (InterpGN) that combines an interpretable expert with a deep neural network (DNN) expert. InterpGN uses a novel gating function to decide whether to use the interpretable expert's prediction or to rely on the DNN's expertise (as likely needed on challenging samples). Our interpretable expert, termed the Shapelet Bottleneck Model (SBM), introduces a variant of the Shapelet Transform (Lines et al., 2012) to build expressive yet interpretable predicates based on learned shapelets (Ye & Keogh, 2011) such as the patterns in Figure 1 (left). Our interpretable expert holds several advantages over existing methods such as fewer parameters than neuro-symbolic method NSTSC, improved shapelet selection due to our Shapelet Transform, and better accuracy due to gating on challenging samples.

Our main **contributions** are summarized as follows: (1) a novel gating function that assigns samples to experts based on the confidence level of the interpretable expert, (2) a novel variant of the Shapelet Transform that improves interpretability compared to existing shapelet-based methods, and (3) quantitative metrics for interpretability and shapelet quality, where we show that our models improve in both metrics over existing shapelet-learning formulations. We further demonstrate that InterpGN outperforms state-of-the-art methods on the UEA multivariate TS classification archive (Bagnall et al., 2018), illustrate the interpretabilityof InterpGN on multivariate TS classification datasets, and FIX
finally apply our framework on a real-world healthcare dataset, MIMIC-III (Johnson et al., 2016).

2 Related Work

Machine Learning Methods for TS Analysis Classical deep learning models such as Multilayer Perceptron (MLP), Fully Convolutional Network (FCN), and Residual Network (ResNet) (Wang

et al., 2017) are usually considered as baselines. ROCKET (Dempster et al., 2020) uses random convolution kernels with various lengths to transform TS data and trains a linear classifier. Another direction is representation learning that uses unsupervised approaches to learn from positive and negative samples (Franceschi et al., 2019). For instance, TapNet (Zhang et al., 2020) proposes an attention prototype network to learn multivariate TS representations and address the issue of limited labeled data. Time Series Transformer (TST) (Zerveas et al., 2021) reconstructs TS from masked data to learn a pre-trained model that can be used for multiple types of downstream tasks. Recent works also find that when combined with deep neural networks such as Transformers (Vaswani et al., 2017), the patch-based modeling, which segments TS into channel-independent patches, is more effective than timestamp-based modeling in various tasks (Zuo et al., 2023; Nie et al., 2023; Wu et al., 2023). Although the above methods may achieve state-of-the-art performance, they lack interpretability.

Interpretable Methods Pattern-based methods usually have some level of interpretability. (Zhao et al., 2023) surveys many methods for interpretable TS classification. A subset of pattern-based methods use shapelets, defined as discriminatory subsequences of TS data (Ye & Keogh, 2011) selected based on information gain. ShapeNet (Li et al., 2021) learns embeddings that encode subsequences with different lengths into a unified space using triplet loss, and then selects the most representative shapelets to use with Shapelet Transforms. Shapelets can also be learned using gradient-based methods (Grabocka et al., 2014), relaxing the definition of shapelets as sequences with certain patterns. However, with the original formulation, the learned shapelets have poor quality as they may not look similar to the actual subsequences. ADSN (Ma et al., 2020) improves shapelet quality using adversarial training. ShapeConv (Qu et al., 2024) initializes the shapelets as the cluster means of TS subsequence and uses an additional regularization to keep shapelets close to the actual subsequence during training. Besides shapelet-based methods, a recent pattern-based method RLPAM (Gao et al., 2022) first transform TS to a sequence of patterns and uses reinforcement learning to select the most informative patterns for classification.

3 Problem Formulations

Notation Let $\mathcal{D} = \{(x_i, y_i)|i = 1, \ldots, N\}$ denotes a TS classification dataset with N samples, where $x_i \in \mathbb{R}^{M\times T}$ is a TS sample and $y_i \in \{1, \ldots, C\}$ is the class label. Here, M is the number of variables, T is the length in timestamps, and C is the number of categories. A multivariate TS sample x_i can be viewed as a set of univariate TS samples where $x_i^m \in \mathbb{R}^T$ denotes the TS of the mth variable. $x_{i,t_1:t_2}^m$ denotes a subsequence of x_i^m between timestamps t_1 and t_2.

Shapelets Shapelets were originally defined as discriminative TS subsequences to distinguish different categories (Ye & Keogh, 2011). Learning Time-series Shapelets (LTS) (Grabocka et al., 2014) combines Shapelet Transform with gradient-based optimization to learn a set of shapelets from scratch, where the definition of shapelets is relaxed to be short sequences with certain patterns. In this work, we follow the definition of LTS where the shapelets are the model's parameter to train.

Shapelet-based TS Modeling Independently modeling each channel of a multivariate TS has been demonstrated to be an effective approach (Wu et al., 2023; Nie et al., 2023). In this paper, we consider a similar approach by formulating univariate shapelets for each variable separately. Let

$$\mathcal{S} = \{s_k^{m,l}|k = 1, \ldots, K; m = 1, \ldots, M; l \in L\}$$

denote a set of shapelets, where $s_k^{m,l} \in \mathbb{R}^l$ denotes a shapelet on the mth channel with length l and index k, i.e., we learn K shapelets for each possible length and channel. In this paper, we consider shapelets with multiple lengths where $L = \{\max(\lceil \delta T \rceil, 3)|\delta = 0.05, 0.1, 0.2, 0.3, 0.5, 0.8\}$. Therefore, $\mathcal{S}$ has a total of $MK|L|$ shapelets.

Interpretability Existing methods gain different levels of interpretability by inputting interpretable features (Zuo et al., 2023) into a simple model such as a linear layer (Ma et al., 2020; Qu et al., 2024) or SVM (Li et al., 2021). However, such approaches usually fail to provide explanations of their predictions based on distances features. For the interpretable expert, we build logical predicates using shapelets and the classifier directly provides rule-like explanations. Combining interpretable features with logic allows this approach to select essential shapelets since model weights associated with shapelets represent corresponding importance to predictions (Riegel et al., 2020).

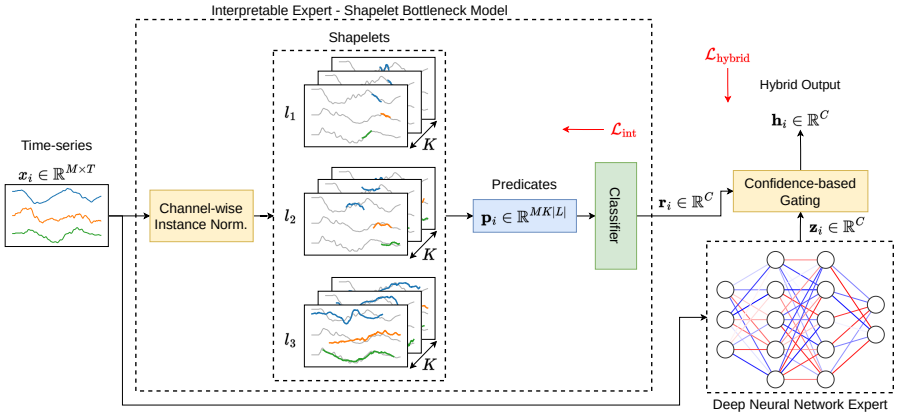

Figure 2: Overview of InterpGN.

4 The Mixture-of-Experts Framework: InterpGN

In this section, we present the details of Interpretability Gated Networks (InterpGN). We first discuss the proposed variant of Shapelet Transforms to build logical predicates and the formulations of the Shapelet Bottleneck Model (SBM), and then discuss how explanations can be derived from SBM. Lastly, we present the novel gating function used by InterpGN along with the training procedure. An overview of InterpGN is given in Figure 2.

4.1 Building Logical Predicates using Shapelets

A straightforward way to express predictions with logical classifiers is to use predicates built on features such as distances. Mueen et al. (2011) constructed a logical predicate with a threshold distance; however, when combined with LTS, we find this approach reduces shapelet quality (essential shapelets are not similar to the TS) as well as interpretability (notion of distance can vary across datasets) since the threshold distance does not directly reflect the existence of a shapelet (see Figure 3 for an example). Therefore, analogous to concepts in CBM, we view shapelets as interpretable concepts for TS and build logical predicates directly from shapelet distances. Consider the distance between $s_k^{m,l}$ and x_i^m defined as:

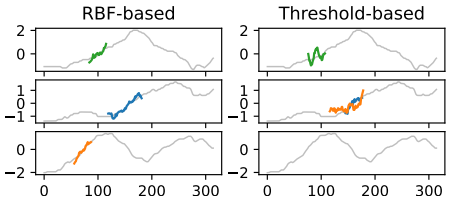

Figure 3: Comparison between shapelets learned by (left) radial basis function (RBF) based predicates and (right) threshold based predicates. The three most important shapelets are visualized.

$$d_{i,k}^{m,l} = \min_{t=1,\ldots,T-l} \texttt{dist}(s_k^{m,l}, x_{i,t:t+l}^m), \tag{1}$$

where $\texttt{dist}(s_k^{m,l}, x_{i,t:t+l}^m)$ is the Euclidean distance between the two sequences. We introduce a variant of the Shapelet Transform, formally defined by

$$p_{i,k}^{m,l} = \max_{t=1\ldots,T-l} e^{-\left(\epsilon \cdot \texttt{dist}(x_{i,t:t+l}^m, s_k^{m,l})\right)^2} \tag{2}$$

using a Gaussian radial basis function on the distance to measure the likelihood that $s_k^{m,l}$ exists in x_i^m, where ϵ is a scaling parameter that controls the steepness of the kernel. We say that the set of shapelets $\mathcal{S}$ transforms each sample $x_i \in \mathcal{D}$ to predicates $\mathbf{p}_i \in \mathbb{R}^{MK|L|}$, where $\mathbf{p}_i = \left[p_{i,k}^{m,l} \mid k = 1, \ldots, K;\ m = 1, \ldots, M;\ l \in L\right]$.

4.2 SHAPELET BOTTLENECK MODEL - THE INTERPRETABLE EXPERT

When constructing the SBM, we adopt a similar approach to LTS and CBM to preserve interpretability and produce rule-like classifiers. Formally, the predicates $\mathbf{p}_i$ are fed into a linear layer to compute the outputs

$$r_{i,c} = \sum_{k=1,\ldots,K;m=1,\ldots,M;l\in L} w_{c,k}^{m,l}\, p_{i,k}^{m,l},\ \forall c \in \{1,\ldots,C\}. \tag{3}$$

The SBM's output is $\mathbf{r}_i \in \mathbb{R}^C = [r_{i,1},\ldots,r_{i,C}]$. An overview of SBM is given in Figure 2. Note that the different shapelet lengths are illustrated vertically under the Shapelet Bottleneck; each row allows shapelets of length l across all variables.

Training SBM is end-to-end differentiable and trained using gradient-based optimization. The parameters to be trained include the linear classifier weights $w_{c,k}^{m,l}$ and the shapelets $s_k^{m,l}$, both of which are randomly initialized. In practice, gradients of the `max` operator in Equation 2 can be substituted by gradients of `softmax` using straight-through estimation. The objective function contains the following three loss functions: NEW

- Classification loss: softmax cross-entropy loss $\mathcal{L}_{\text{ce}}$ on $(\mathbf{r_i}, y_i)$,
- Shapelet diversity loss (Ma et al., 2020) to regulate learning redundant shapelets:

$$\mathcal{L}_{\text{div}} = \frac{1}{2KM|L|} \sum_{m=1}^{M} \sum_{l\in L} \sum_{k_1=1}^{K} \sum_{\substack{k_2=1 \\ k_2\neq k_1}}^{K} e^{-\|s_{k_1}^{m,l} - s_{k_2}^{m,l}\|_2}, \tag{4}$$

- L1 regularization $\mathcal{L}_{\text{reg}}$ on the classifier weights $w_{c,k}^{m,l}$ to encourage sparsity, select the most informative concepts, and produce simple classifiers.

The overall loss function is

$$\mathcal{L}_{\text{int}} = \mathcal{L}_{\text{ce}} + \lambda_{\text{div}}\mathcal{L}_{\text{div}} + \lambda_{\text{reg}}\mathcal{L}_{\text{reg}}, \tag{5}$$

where λ_{div}, and λ_{reg} are hyperparameters.

4.3 INTERPRETATIONS

A concept probability $p_{i,k}^{m,l}$ is a logical predicate whose value measures the existence of shapelet $s_k^{m,l}$. The linear classifier behaves like weighted linear logic analogous to the operators in Riegel et al. (2020), where weights $w_{c,k}^{m,l}$ specify the importance of shapelet $s_k^{m,l}$ to class c. We propose two ways to interpret the model.

Local Explainability Local explanations answer why the classification decision for a sample x_i was made. In SBM, the explanation has the form of "sample x_i belongs to class c because x_i contains shapelet $s_k^{m,l}$", whose corresponding $w_{c,k}^{m,l} p_{i,k}^{m,l}$ is significant. Consider Figure 1 in the Introduction where we visualize the two shapelets with the largest $w_{c,k}^{m,l} p_{i,k}^{m,l}$ for each class. Such interpretations allow us to visually validate the correctness of learned shapelets and classifiers. Note that, to the best of our knowledge, most existing shapelet-based methods (Qu et al., 2024) and post-hoc explanation methods (Queen et al., 2023) only provide local explainability.

Global Explainability Global explanations provide knowledge about the classification problem, expressed in SBM by inductive logics without pertaining to particular samples. SBM offers the following global explanation: (1) $w_{c,k}^{m,\delta} > 0$: samples in class c *should* contain $s_k^{m,\delta}$, (2) $w_{c,k}^{m,\delta} = 0$: $s_k^{m,\delta}$ is unrelated to class c, (3) $w_{c,k}^{m,\delta} < 0$: samples in class c *should not* contain $s_k^{m,\delta}$.

Most figures in this paper visualize shapelets with the highest weights in the linear classifier, validating the correctness of the global explanation. For some challenging tasks, we use local explanations to provide visually better explanations for specific samples. Note the difference between local and global explainability: local explanations discuss what *does* occur in a sample whereas global explanations discuss what *should* occur in a sample.

4.4 Mixture-of-Experts Gating

In the previous section, the shapelet bottleneck transforms TS into low-dimensional representations in the form of logical predicates. While the `max` operator in Equation (2) makes the classifier more interpretable, it also reduces expressiveness. For example, the predicates can only measure the existence of shapelets but lose information about the number of occurrences and corresponding timestamps. In TS with discriminative features in other domains, such as the frequency domain instead of the time domain, the shapelet bottleneck may not capture essential features for classification. To address this limitation, we employ a Mixture-of-Experts approach to build a partially-interpretable hybrid model.

A Mixture-of-Experts (MoE) combines the output of multiple expert models with a gating network (Shazeer et al., 2017). Experts have different structures to capture different aspects of the data and the gating network assigns the work to the experts. IME (Ismail et al., 2023) views a simple model (such as linear regression or soft decision tree) as an interpretable gating network. From a different perspective, the interpretable expert itself can serve as the gating network, which reduce the number of parameters and improves interpretability. We introduce a gating function to assign the work to experts based on the confidence level of the interpretable expert. FIX

The outputs $\mathbf{r}_i$ minimizes $\mathcal{L}_{\text{ce}}$ during training. Denote $\hat{\mathbf{r}}_i = \texttt{softmax}(\mathbf{r}_i)$ with components $\hat{r}_{i,c}$ corresponding to Equation (3). Then the optimal $\hat{\mathbf{r}}_i$ is a one-hot vector with $\hat{r}_{i,c} = 1$ if $y_i = c$. Diversity of $\hat{r}_{i,c}$ thus measures confidence of the model. When combining an interpretable model and a DNN with MoE, the use of DNN should be inverse proportional to the confidence level of the interpretable model to maximize interpretability. Therefore, we design the gating function

$$\eta(x_i) = \frac{C \cdot \sum_{c=1}^{C} (\hat{r}_{i,c})^2 - 1}{C - 1}, \tag{6}$$

which is a modified Gini Index that measures the diversity of variables in $\hat{\mathbf{r}}_i$. Intuitively, $\eta(x_i) = 0$ when values in $\hat{\mathbf{r}}_i$ are identical, and $\eta(x_i) = 1$ when $\hat{\mathbf{r}}_i$ is a one-hot vector. During training, the output of the hybrid model is then a mixture of the outputs of the interpretable expert and the DNN with ratio $\eta(x_i)$:

$$\mathbf{h}_i = \mathbf{r}_i \cdot \eta(x_i) + \mathbf{z}_i \cdot (1 - \eta(x_i)), \tag{7}$$

where $\mathbf{z}_i$ is the output of the DNN with input x_i. During inference, we activate only the SBM and discard the DNN if the confidence of SBM is high. Specifically, given a gating value $\underline{\eta}$, we set $\eta(x_i) = 1$ if $\eta(x_1) > \underline{\eta}$. NEW

4.5 Training of InterpGN

The overall objective of the InterpGN framework is to minimize $\mathcal{L}_{\text{hybrid}} = \beta\mathcal{L}_{\text{int}} + \bar{\mathcal{L}}_{\text{ce}}$. Here, $\bar{\mathcal{L}}_{\text{ce}}$ is another softmax cross-entropy loss on $(\mathbf{h}_i, y_i)$ to optimize the overall performance of the hybrid model. $\beta \in [0, 1]$ is a scalar to weight the training of the interpretable expert, which is set to be either a constant hyperparameter or decaying with a cosine schedule. Intuitively, the $\mathcal{L}_{\text{int}}$ term directly optimizes the SBM component, which ensure that the SBM is actively encouraged to find meaningful shapelets. This design prevents InterpGN from collapsing into a pure DNN model whenever the shapelet-based features are useful (see Figure 22 and Figure 23). The hybrid model is still end-to-end differentiable and trained using gradient-based optimizations methods. NEW

5 Experiments

We first compare InterpGN against various methods on the UEA multivariate TS classification archive, presenting insights gained from visualizing concept representations. Results from SBM without the additional expert are also given. We then demonstrate the benefits of our models on the real-world application of in-hospital mortality early prediction (Harutyunyan et al., 2019) using the MIMIC III dataset. We conclude with ablation studies on the effects of each component in our model. As a basic InterpGN design, we combine the SBM with a Fully Convolutional Network (FCN) since it has best performance among the three basic deep models for TS classification (Wang et al., 2017). Details of the experimental setup are provided in Appendix A.

Table 1: Comparison on 30 datasets from the UEA archive. The best accuracy for each dataset is marked with bold, the second-best is marked with italic, and the third-best is marked with underline.

	Classical		Deep Learning						With Interpretable Features			Ours	
Dataset	STRF	DTW	FCN	TS2Vec	TimesNet	TST	PatchTST	SVP-T	ShapeNet	RLPAM	ShapeConv	SBM	InterpGN
Avg. Accuracy	0.645	0.650	0.740	0.704	0.710	0.709	0.669	0.730	0.697	0.740	*0.743*	0.718	**0.746**
Avg. Rank	9.633	9.000	*4.800*	7.400	7.750	6.926	9.926	5.000	6.267	5.300	5.533	5.633	**4.133**
Num. Top-1	2	1	6	1	0	5	0	5	2	**7**	2	3	**7**
Num. Top-3	2	1	**14**	2	4	8	2	13	7	**14**	10	10	12
Wins/Draws	27	27	18	26	20	18	24	18	22	18	19	20	-
Losses	3	2	12	4	8	9	3	12	8	12	11	10	-
Wilcoxon p-value	0.000	0.000	0.367	0.000	0.000	0.002	0.000	0.392	0.026	0.299	0.084	0.080	-

5.1 Multivariate Time Series Classification

First, we evaluate the performance of InterpGN on 30 datasets from the UEA multivariate TS classification archive and compare with baseline methods including (1) classical search-based method: Shapelet Transform with Random Forest Classifier (STRF) and DTW (Chen et al., 2013), (2) black-box deep learning methods: FCN (Wang et al., 2017), TS2Vec (Yue et al., 2022), TimesNet (Wu et al., 2023), TST (Zerveas et al., 2021), PatchTST (Nie et al., 2023), SVP-T (Zuo et al., 2023), and (3) methods with interpretable features: ShapeNet (Li et al., 2021), RLPAM (Gao et al., 2022), ShapeConv (Qu et al., 2024). FIX

Table 1 presents average classification accuracy across the UEA datasets; the full results are included in Table 6 of Appendix B.1. Based on the average rank across the 30 datasets, InterpGN outperforms the baseline methods and SBM achieves comparable performance without help from the FCN.

5.1.1 Interpretability

In addition to its effective performance, SBM provides interpretable logical classifiers. Figure 4 visualizes shapelets learned by SBM on a multivariate TS dataset from global explanations, where the blue shapelets have the highest positive weights and the red shapelets have the lowest negative weights. Figure 4 visually confirms that the models capture discriminative shapelet features.

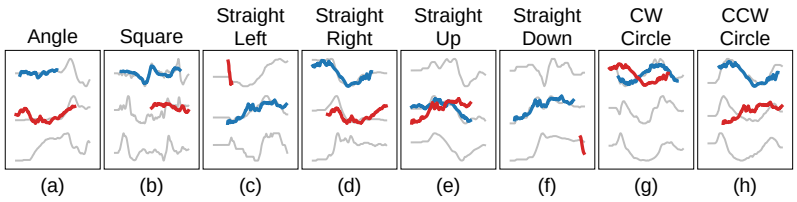

Figure 4: Visualization of the *UGL* dataset from the UEA archive with accelerometer readings of eight gestures. For example, in (g), the classifier can be interpreted as: a "CW Circle" gesture should contain the blue shapelet but not the red shapelet in channel 1.

5.1.2 Shapelet Bottleneck Representation

We explore the effectiveness of the shapelet predicates by viewing probabilities $\mathbf{p}_i$ as representations for TS data. Figure 5 displays the EP dataset using the dimensionality reduction technique t-SNE (van der Maaten & Hinton, 2008). Representations learned by SBM and InterpGN are clearly more separable than the raw TS data. While a few samples are mixed into incorrect clusters (e.g., blue mixed into green), the DNN in the InterpGN model can make corrections and result in better accuracy than SBM. Shading intensity of data points in Figure 5 (c) represents $\eta(x_i)$. Intuitively, predictions FIX of shaded points are interpretable as they are based on SBM while lighter points rely more on the DNN. We observe that most transparent points lie along the cluster boundaries, meaning InterpGN learns to use interpretable logical classifier for easier-to-classify samples while relying on the DNN to classify the difficult boundary samples which can be identified as requiring additional expertise. In Figure 17, we further present the behavior of InterpGN by visualizing the distribution of $\eta(x_i)$. We can conclude that the predictions of InterpGN is consistent with SBM when $\eta(x_i)$ is high, preserving interpretability for those samples.

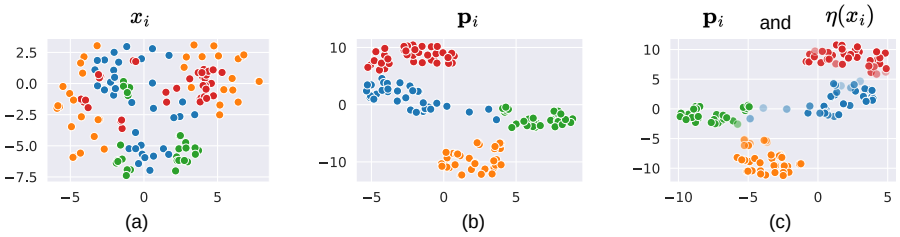

Figure 5: t-SNE dimensionality reduction of (a) raw data x_i, (b) $\mathbf{p}_i$ of SBM, and (c) $\mathbf{p}_i$ of InterpGN on the *EP* dataset. Each color represents samples with a specific label. Samples with low $\eta(x_i)$ from InterpGN lie on the boundary, i.e., are more difficult to predict and can benefit from additional expertise.

5.2 Predicting In-hospital Mortality

The MIMIC-III dataset contains electronic healthcare records from ICU patients. We follow the procedure in (Harutyunyan et al., 2019) to preprocess and generate data to predict in-hospital mortality based on patient records from the first 48 hours after entering an ICU. Setup details are provided in Appendix A.2. Table 2 shows results illustrating how InterpGN helps SBM on the difficult samples.

Interpretability Clinical records from the MIMIC-III dataset are challenging due to sample diversity and missing values. Figure 6 highlights an example of local explanations on two samples. For better representation, we visualize the five most essential shapelets on their corresponding channels and omit other channels. The model captures long-term discriminative trends in three channels, HR, MBP and OS. The shapelets and classifier can be interpreted as: the first patient passed away due to decreasing HR, increasing MBP, and drop in OS; whereas the second survived because of increasing HR after a local drop, rapid decrease in MBP, and steady OS. In real-world scenarios, these interpretations could bring more insights to clinical applications than DNNs that only provide black-box predictions.

Table 2: Results for in-hospital mortality predication on the MIMIC-III dataset.

Metric	STRF	FCN	SBM	InterpGN
Accuracy	0.653	0.693	0.658	**0.703**
F1	0.639	**0.675**	0.657	0.657
Recall	0.615	0.634	**0.657**	0.569
Precision	0.666	0.734	0.659	**0.784**
ROC-AUC	0.653	0.698	0.658	**0.703**

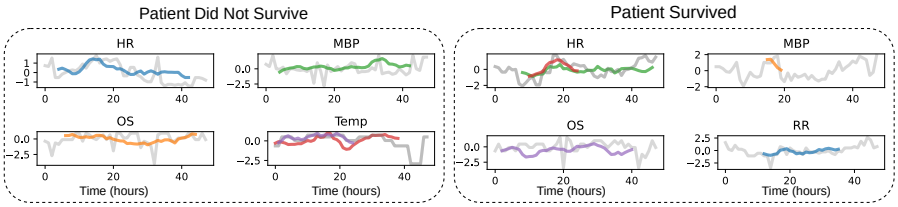

Figure 6: Local explanations of SBM for in-hospital mortality predication. The variables in the figure are: Heart Rate (HR), Mean Blood Pressure (MBP), Oxygen Saturation (OS), Respiratory Rate (RR), and Temperature (Temp).

5.3 Effects of Hyperparameters on Interpretability and Shapelet Quality

Analogous to the results presented in Figure 1 and Section 5.1.1, existing interpretable models mainly demonstrate qualitative results on interpretabilityby visualizing the interpretable features (Ma et al., 2020; Qu et al., 2024). However, there remains a lack of quantitative metrics to measure the level of interpretability and quality of features. Therefore, we introduce two additional metrics to quantitatively assess the interpretable models. FIX

Interpretability metric: Naturally, the prediction from the model is considered more interpretable if fewer features are needed to simulate and understand the prediction. With a linear classifier taking logical predicates as inputs, interpretability of SBM can be measured by the sparsity of the classifier weights since fewer shapelets contribute to the prediction as weight sparsity increases. As a metric for sparsity, we choose three empirical thresholds and compute the ratio of weights above each threshold. Formally, the sparsity metrics are defined as

$$\text{ratio} = \frac{1}{|\mathcal{W}|} \sum_{w \in \mathcal{W}} \mathbb{1}(|w| > t), \ \textbf{for } t \in \{1, 0.5, 0.1\}. \tag{8}$$

Additionally, as a relative sparsity measurement, we also compute the Gini coefficient of $|w|$. NEW

Shapelet quality metric: In order to produce reliable representations in shapelet-based models, the shaplets need to be "close" to the actual TS subsequences. Therefore, shapelet quality can be measured by shapelet distances (defined by Equation 1). In a prediction, more important shapelets should be expected to have higher quality. Therefore, for our SBM, the shapelet quality metric is defined as

$$\text{shapelet error} = \frac{\mathbb{1}(\hat{y}_i = y_i)}{MK|L|} \sum_{m=1}^{M} \sum_{l \in L} \sum_{k=1}^{K} \max(0, w_{y_i,k}^{m,l}) d(x_i^m, s_k^{m,l}), \ (x_i, y_i) \in \mathcal{D}_{\text{test}} \tag{9}$$

which measures the shapelet distances for samples that are correctly classified, averaged over all shapelets in SBM and weighted by their corresponding classifier weight if $w_{c,k}^{m,l} > 0$. Low shapelet error reflects that the essential shapelets for the prediction are close to the actual TS subsequences which represent high shapelet quality.

Results and Analysis We conduct an ablation study on the effect of hyperparameters on classification accuracy, interpretability, shapelet quality, and interpretable expert utility. Details for the ablation study setup are summarized in Appendix A.4. The results are summarized in Tables 7, 8, 9 and Figures 18, 19, 20, 21, which lead to the following respective conclusions:

• **Number of shapelet** K determines the expressiveness of SBM. Table 7 shows that increasing K improving accuracy while additionally improving shapelet quality since the shapelet could capture more sample-specific patterns. Although the classifier weights also become sparser, the absolute number of weights above the threshold values may also increase. Therefore, the effect of K on interpretability may not be clearly concluded. In InterpGN, the SBM utility rate η also increase as K increase since the SBM becomes more expressive.

• **Schedule of of loss weighting** β controls the training of the interpretable expert in InterpGN. If β decays with a cosine schedule, the SBM no longer trains on samples that cannot be confidently predicted as the models get trained. Table 8 shows that, compared to a constant schedule, models trained with the cosine schedule result in slightly worse accuracy but improve in both shapelet quality and interpretability since the SBMs focus more on samples where shapelet features are useful. As less samples are fitted, η also decreases.

• **Predicate type** defines the method of building logical predicates from shapelet distances. In our models, the SBM uses the RBF predicates defined in Equation 2. Another commonly used formulation is a linear predicate (Mueen et al., 2011; Yan et al., 2022) which computes threshold-based predicates by $p_{i,k}^{m,l} = \texttt{sigmoid}(c_k^{m,l} - d_{i,k}^{m,l})$ where $c_k^{m,l}$ is the threshold value to learn. Table 9 shows that our RBF predicates outperform linear predicates in accuracy, shapelet quality, and interpretability.

• ϵ **affects the steepness of the RBF kernels**. A large ϵ defines a tight kernel and pushes the shapelet to be close to the TS data. Figure 18 demonstrates that increasing ϵ improves shapelet quality in the SBM but significantly reduces the accuracy for $\epsilon \geq 5$. $\epsilon = 1$ offers the best balance between shapelet quality and accuracy.

• **Weight regularization** λ_{reg} affects the sparsity of classifier weights and the number of shapelets contributing to the predictions. Figure 21 shows that increasing λ_{reg} improves interpretability without significantly affecting the accuracy for $0 \leq \lambda_{\text{reg}} \leq 1$.

• **Shapelet diversity regularization** λ_{div} encourages learning different shapelets. Figure 20 leads us to conclude that λ_{div} does not have a significant effect on the three metrics.

• **Gating value** $\underline{\eta}$ controls the threshold of discarding the DNN during inference. Prediction of samples with $\eta(x_i) > \underline{\eta}$ only rely on the SBM, maximizing their interpretability. Figure 19 shows that reducing the gating value results in slight degrade in accuracy, where the difference in average accuracy between using $\underline{\eta} = 0.5$ and $\underline{\eta} = 1$ is 0.004. NEW

Finally, we perform additional ablation studies on the architecture of the DNN expert within the InterpGN model. Specifically, we experiment with four supervised deep learning models: FCN, Transformer, PatchTST, and TimesNet. Table 3 reports the average test accuracy and utility for these cases on a subset of the UEA datasets. Among the tested architectures, InterpGN with FCN achieves the highest accuracy on most datasets. Interestingly, we observe that the choice of DNN significantly affects eta for each dataset, reflecting the compatibility between the SBM and the DNN. This highlights a complex relationship between the features learned by the SBM and those captured by different DNN architectures, which may worth more in-depth study. NEW

Table 3: Ablation on the architecture of the DNN expert in InterpGN. The best performance for each dataset is highlighted with bold.

DNN Expert of InterpGN:	FCN		Transformer		PatchTST		TimesNet	
Dataset	accu.	η	accu.	η	accu.	η	accu.	η
EthanolConcentration	0.281	0.014	**0.300**	0.446	0.276	0.612	0.277	0.001
FaceDetection	0.658	0.708	0.663	0.664	0.661	0.619	**0.682**	0.638
Handwriting	**0.612**	0.011	0.268	0.020	0.238	0.012	0.319	0.012
Heartbeat	**0.762**	0.629	0.737	0.435	0.735	0.898	0.741	0.478
JapaneseVowels	**0.989**	0.818	0.982	0.871	0.944	0.825	0.972	0.806
SelfRegulationSCP1	**0.901**	0.520	0.881	0.097	0.835	0.169	0.896	0.274
SelfRegulationSCP2	**0.571**	0.056	0.556	0.361	0.556	0.496	0.570	0.001
SpokenArabicDigits	**0.997**	0.976	0.994	0.986	0.994	0.986	0.995	0.977
UWaveGestureLibrary	**0.912**	0.504	0.814	0.068	0.799	0.224	0.850	0.643

6 Conclusion and Limitations

In this paper, we address the limitations of existing TS classification methods. We introduce InterpGN, which leverages the trade-off between interpretability and performance. We present a variant of the Shapelet Transform to build logical predicates from shapelets and propose a novel gating function design based on confidence of the interpretable model. Our experiments demonstrate that InterpGN outperforms existing methods while preserving interpretability for most samples. We also interpreted and analyzed patterns and classifiers learned by the models on various datasets, and applied our models to the MIMIC-III dataset to provide interpretable logics and discover knowledge on a real-world task.

We note two **limitations** of our study. Firstly, in some classification rules, the most important shapelet for class c may not look similar to subsequences of TS in class c. Such rules tend to have interpretations with form "x_i belongs to class c since it does not contain the essential shapelets for $c' \neq c$" or "x_i belongs to class c since other $c' \neq c$ do not contain shapelet s". For example, the blue shapelet in Figure 4 (a) may not capture the essential trend for the "Angle" movement but it can still be correctly categorized since it does not contain the essential shapelets for other categories. Secondly, note that we have studied a simple design which includes one interpretable expert and one DNN. Analogous to the MoE (Shazeer et al., 2017) framework, InterpGN can scale up by integrating more experts. For example, multiple interpretable models can be included using a hierarchical gating approach, while multiple DNN models can be combined using the original MoE approach. Additionally, we only consider a linear classifier since it is the easiest model to interpret and provides importance to rate the shapelets. Advanced interpretable structures, such as attention-based methods or graph neural networks, could effectively capture additional information about TS data, such as dependencies between shapelets from different channels. We present a preliminary study of two non-linear classifiers in Appendix C.2 and reserve more exploration for future work. FIX

REFERENCES

Talal AA Abdullah, Mohd Soperi Mohd Zahid, Waleed Ali, and Shahab Ul Hassan. B-lime: An improvement of lime for interpretable deep learning classification of cardiac arrhythmia from ecg signals. In *Processes*, 2023.

David Alvarez Melis and Tommi Jaakkola. Towards robust interpretability with self-explaining neural networks. *Advances in neural information processing systems*, 31, 2018.

Saira Aziz, Sajid Ahmed, and Mohamed-Slim Alouini. Ecg-based machine-learning algorithms for heartbeat classification. In *Nature: Scientific Reports*, volume 11, 2021.

Anthony Bagnall, Hoang Anh Dau, Jason Lines, Michael Flynn, James Large, Aaron Bostrom, Paul Southam, and Eamonn Keogh. The UEA multivariate time series classification archive, 2018. *arXiv preprint arXiv:1811.00075*, 2018.

Yanping Chen, Bing Hu, Eamonn Keogh, and Gustavo EAPA Batista. DTW-D: time series semi-supervised learning from a single example. In *Proceedings of the 19th ACM SIGKDD international conference on Knowledge discovery and data mining*, pp. 383–391, 2013.

Angus Dempster, François Petitjean, and Geoffrey I Webb. Rocket: exceptionally fast and accurate time series classification using random convolutional kernels. *Data Mining and Knowledge Discovery*, 34(5):1454–1495, 2020.

Jean-Yves Franceschi, Aymeric Dieuleveut, and Martin Jaggi. Unsupervised scalable representation learning for multivariate time series. *Advances in neural information processing systems*, 32, 2019.

Ge Gao, Qitong Gao, Xi Yang, Miroslav Pajic, and Min Chi. A reinforcement learning-informed pattern mining framework for multivariate time series classification. In *31st International Joint Conference on Artificial Intelligence (IJCAI)*, 2022.

Josif Grabocka, Nicolas Schilling, Martin Wistuba, and Lars Schmidt-Thieme. Learning time-series shapelets. In *Proceedings of the 20th ACM SIGKDD international conference on Knowledge discovery and data mining*, pp. 392–401, 2014.

Hrayr Harutyunyan, Hrant Khachatrian, David C Kale, Greg Ver Steeg, and Aram Galstyan. Multitask learning and benchmarking with clinical time series data. *Scientific data*, 6(1):96, 2019.

Marton Havasi, Sonali Parbhoo, and Finale Doshi-Velez. Addressing leakage in concept bottleneck models. *Advances in Neural Information Processing Systems*, 35:23386–23397, 2022.

Aya Abdelsalam Ismail, Sercan O Arik, Jinsung Yoon, Ankur Taly, Soheil Feizi, and Tomas Pfister. Interpretable mixture of experts. *Transactions on Machine Learning Research*, 2023. ISSN 2835-8856.

Alistair EW Johnson, Tom J Pollard, Lu Shen, Li-wei H Lehman, Mengling Feng, Mohammad Ghassemi, Benjamin Moody, Peter Szolovits, Leo Anthony Celi, and Roger G Mark. Data descriptor: Mimic-iii, a freely accessible critical care database. *Scientific data*, 3(160035):1–9, 2016.

Pang Wei Koh, Thao Nguyen, Yew Siang Tang, Stephen Mussmann, Emma Pierson, Been Kim, and Percy Liang. Concept bottleneck models. In *International conference on machine learning*, pp. 5338–5348. PMLR, 2020.

Seungeon Lee, Xiting Wang, Sungwon Han, Xiaoyuan Yi, Xing Xie, and Meeyoung Cha. Self-explaining deep models with logic rule reasoning. *Advances in Neural Information Processing Systems*, 35:3203–3216, 2022.

Guozhong Li, Byron Choi, Jianliang Xu, Sourav S Bhowmick, Kwok-Pan Chun, and Grace Lai-Hung Wong. Shapenet: A shapelet-neural network approach for multivariate time series classification. In *Proceedings of the AAAI conference on artificial intelligence*, volume 35, pp. 8375–8383, 2021.

Jason Lines, Luke M Davis, Jon Hills, and Anthony Bagnall. A shapelet transform for time series classification. In *Proceedings of the 18th ACM SIGKDD international conference on Knowledge discovery and data mining*, pp. 289–297, 2012.

Qianli Ma, Wanqing Zhuang, Sen Li, Desen Huang, and Garrison Cottrell. Adversarial dynamic shapelet networks. In *Proceedings of the AAAI conference on artificial intelligence*, volume 34, pp. 5069–5076, 2020.

Noushin Mehdipour, Cristian-Ioan Vasile, and Calin Belta. Specifying user preferences using weighted signal temporal logic. *IEEE Control Systems Letters*, 5(6):2006–2011, 2021. doi: 10.1109/LCSYS.2020.3047362.

Abdullah Mueen, Eamonn Keogh, and Neal Young. Logical-shapelets: an expressive primitive for time series classification. In *Proceedings of the 17th ACM SIGKDD international conference on Knowledge discovery and data mining*, pp. 1154–1162, 2011.

I. Neves, D. Folgado, S. Santos, M. Barandas, A. Campagner, L. Ronzio, F. Cabitza, and H. Gamboa. Interpretable heartbeat classification using local model-agnostic explanations on ecgs. In *Computers in Biology and Medicine*, 2021.

Yuqi Nie, Nam H Nguyen, Phanwadee Sinthong, and Jayant Kalagnanam. A time series is worth 64 words: Long-term forecasting with transformers. In *The Eleventh International Conference on Learning Representations*, 2023.

Tuomas Oikarinen, Subhro Das, Lam M Nguyen, and Tsui-Wei Weng. Label-free concept bottleneck models. In *The Eleventh International Conference on Learning Representations*, 2022.

Yuzuru Okajima and Kunihiko Sadamasa. Deep neural networks constrained by decision rules. In *Proceedings of the AAAI Conference on Artificial Intelligence*, volume 33, pp. 2496–2505, 2019.

Eric Qu, Yansen Wang, Xufang Luo, Wenqiang He, Kan Ren, and Dongsheng Li. Cnn kernels can be the best shapelets. In *The Twelfth International Conference on Learning Representations*, 2024.

Owen Queen, Tom Hartvigsen, Teddy Koker, Huan He, Theodoros Tsiligkaridis, and Marinka Zitnik. Encoding time-series explanations through self-supervised model behavior consistency. In *Advances in Neural Information Processing Systems*, volume 36, pp. 32129–32159, 2023.

Ryan Riegel, Alexander Gray, Francois Luus, Naweed Khan, Ndivhuwo Makondo, Ismail Yunus Akhalwaya, Haifeng Qian, Ronald Fagin, Francisco Barahona, Udit Sharma, Shajith Ikbal, Hima Karanam, Sumit Neelam, Ankita Likhyani, and Santosh Srivastava. Logical neural networks, 2020.

Noam Shazeer, Azalia Mirhoseini, Krzysztof Maziarz, Andy Davis, Quoc Le, Geoffrey Hinton, and Jeff Dean. Outrageously large neural networks: The sparsely-gated mixture-of-experts layer. In *International Conference on Learning Representations*, 2017.

Laurens van der Maaten and Geoffrey Hinton. Visualizing data using t-sne. In *Journal of Machine Learning Research*, volume 9, pp. 2579–2605, 2008.

Ashish Vaswani, Noam Shazeer, Niki Parmar, Jakob Uszkoreit, Llion Jones, Aidan N Gomez, Lukasz Kaiser, and Illia Polosukhin. Attention is All you Need. In *Advances in Neural Information Processing Systems*, volume 30, 2017.

Zhiguang Wang, Weizhong Yan, and Tim Oates. Time series classification from scratch with deep neural networks: A strong baseline. In *2017 International joint conference on neural networks (IJCNN)*, pp. 1578–1585. IEEE, 2017.

Haixu Wu, Tengge Hu, Yong Liu, Hang Zhou, Jianmin Wang, and Mingsheng Long. Timesnet: Temporal 2d-variation modeling for general time series analysis. In *International Conference on Learning Representations*, 2023.

Ruixuan Yan, Tengfei Ma, Achille Fokoue, Maria Chang, and Agung Julius. Neuro-symbolic models for interpretable time series classification using temporal logic description. In *2022 IEEE International Conference on Data Mining (ICDM)*, pp. 618–627. IEEE, 2022.

Lexiang Ye and Eamonn Keogh. Time series shapelets: a novel technique that allows accurate, interpretable and fast classification. *Data mining and knowledge discovery*, 22:149–182, 2011.

Zhihan Yue, Yujing Wang, Juanyong Duan, Tianmeng Yang, Congrui Huang, Yunhai Tong, and Bixiong Xu. TS2Vec: Towards universal representation of time series. In *Proceedings of the AAAI Conference on Artificial Intelligence*, volume 36, pp. 8980–8987, 2022.

George Zerveas, Srideepika Jayaraman, Dhaval Patel, Anuradha Bhamidipaty, and Carsten Eickhoff. A transformer-based framework for multivariate time series representation learning. In *Proceedings of the 27th ACM SIGKDD conference on knowledge discovery & data mining*, pp. 2114–2124, 2021.

Xuchao Zhang, Yifeng Gao, Jessica Lin, and Chang-Tien Lu. Tapnet: Multivariate time series classification with attentional prototypical network. In *Proceedings of the AAAI conference on artificial intelligence*, volume 34, pp. 6845–6852, 2020.

Ziqi Zhao, Yucheng Shi, Shushan Wu, Fan Yang, Wenzhan Song, and Ninghao Liu. Interpretation of time-series deep models: A survey. *arXiv preprint arXiv:2305.14582*, 2023.

Rundong Zuo, Guozhong Li, Byron Choi, Sourav S Bhowmick, Daphne Ngar-yin Mah, and Grace LH Wong. Svp-t: a shape-level variable-position transformer for multivariate time series classification. In *Proceedings of the AAAI Conference on Artificial Intelligence*, volume 37, pp. 11497–11505, 2023.

A EXPERIMENTAL SETUP

Environment. All the experiments are implemented using Python 3.11 and PyTorch 2.1.2. All the experiments run on a NVIDIA V100-SXM2-32GB GPUs. The SBM and InterpGN are trained on a single GPU. The STRF is implemented using Random Shapelet Transforms from the *Aeon Toolkit* [1] and Random Forest Classifiers from the *Scikit-learn* package, which runs on CPU using 64 threads. FIX

A.1 UEA MULTIVARIATE TIME-SERIES CLASSIFICATION ARCHIVE

The UEA multivariate TS classification archive (Bagnall et al., 2018) contains 30 datasets collected from various domains. Details of the 30 datasets are provided in Table 5. Data preprocessing and training procedure follow the benchmarking repository provided by Wu et al. (2023) [2]. The default hyperparameter to produce results in Table 1 and Table 6 are summarized in Table4. For each dataset, we train the models on the default training split with 5 different random seeds and report the average accuracy on the test split. Statistics on experiment variations could refer to Appendix B.4.

Table 4: Default hyperparameters.

Hyperprameter	Default value
Number of shapelet	$K = 10$
Steepness of RBF kernels	$\epsilon = 1$
Diversity loss weight	$\lambda_{\text{div}} = 0.1$
Sparsity loss weight	$\lambda_{\text{reg}} = 0.1$
β schedule	constant
Inference gating value	$\underline{\eta} = 1$
Optimizer	Adam
Learning rate	0.005
Weight decay	0
Batch size	32

NEW

The metrics in Table 1 and Table 6 are: NEW

- **Avg. Accuracy**: Average test accuracy.
- **Avg. Rank**: Average ranking of the method among all baseline methods.
- **Num. Top-1**: Number of datasets the method performs the best among all baseline methods.
- **Num. Top-3**: Number of datasets the method achieves top-3 accuracy among all baseline datasets.
- **Wins/Draws**: Number of datasets that InterpGN achieves better/same accuracy compared to other baseline methods.
- **Looses**: Number of datasets that InterpGN achieves worse accuracy compared to other baseline methods.
- **P-value**: p-value in the Wilcoxon signed-rank test, which measures if the performance of InterpGN is statistically significant compared to the baseline methods. A small p-value indicates significance, while a large p-value indicates the InterpGN and the baseline method have comparable performance on the UEA datasets.

For the performance of baseline methods, we reproduce STRF, FCN, TimesNet and PatchTST to obtain their performance on the UEA datasets. Other results are obtained from the corresponding paper.

[1] The Aeon Toolkit is available at `www.aeon-toolkit.org`

[2] The benchmarking repository is available at `https://github.com/thuml/Time-Series-Library`

Table 5: Information of the 30 benchmark datasets from the UEA archive.

Dataset	Dataset Code	Train Size N_{train}	Test Size N_{test}	Variables M	Length T	Categories C
ArticularyWordRecognition	AWR	275	300	9	144	25
AtrialFibrillation	AF	15	15	2	640	3
BasicMotions	BM	40	40	6	100	4
CharacterTrajectories	CT	1422	1436	3	119	20
Cricket	CK	108	72	6	1197	12
DuckDuckGeese	DDG	50	50	1345	270	5
ERing	ER	30	270	4	65	6
EigenWorms	EW	128	131	6	17948	5
Epilepsy	EP	137	138	3	206	4
EthanolConcentration	EC	261	263	3	1751	4
FaceDetection	FD	5890	3524	144	62	2
FingerMovements	FM	316	100	28	50	2
HandMovementDirection	HM	160	74	10	400	4
Handwriting	HW	150	580	3	52	26
Heartbeat	HB	204	205	61	405	2
InsectWingbeat	IW	25000	25000	200	22	10
JapaneseVowels	JV	270	370	12	29	9
LSST	LSST	2459	2466	6	36	14
Libras	LB	180	180	2	45	15
MotorImagery	MI	278	100	64	3000	2
NATOPS	NT	180	180	24	51	6
PEMS-SF	PM	267	173	263	144	7
PenDigits	PD	7494	3498	2	8	10
PhonemeSpectra	PH	3315	3353	11	217	39
RacketSports	RS	151	152	6	30	4
SelfRegulationSCP1	SCP1	268	293	6	896	2
SelfRegulationSCP2	SCP2	200	180	7	1152	2
SpokenArabicDigits	SAD	6599	2199	13	93	10
StandWalkJump	SWJ	12	15	4	2500	3
UWaveGestureLibrary	UGL	120	320	3	315	8

A.2 Predicting In-hospital Mortality on MIMIC-III

From the original MIMIC-III dataset, we first extract time-series and impute missing values using the method proposed by Harutyunyan et al. (2019). For predicting in-hospital mortality, the data is highly imbalance, with more than 80% positive samples (patient survived). Therefore we randomly select a subset of 1500 positive and 1500 negative samples to evaluate our models. A sample in the dataset is a TS with $M = 9$ and $T = 48$. We further divide the subset into 80% training and 20% validation to evaluate the performance using 5-fold cross validation. Omitting categorical variables in the MIMIC-III datasets, the TS data has the following 9 variabels:

1. Diastolic blood pressure (DBP),
2. Fraction inspired oxygen (FIO),
3. Heart Rate (HR),
4. Mean blood pressure (MBP),
5. Oxygen saturation (OS),
6. Respiratory rate (RR),
7. Systolic blood pressure (SBP),
8. Temperature (Temp),
9. Glucose (Glu).

A.3 Limitation in Implementation

When combining shapelet learning with modern deep learning frameworks such as PyTorch, the learning suffers from a memory overhead. Intuitively, the transformations in Equation 1 and Equation 2 slide $s_k^{m,l}$ over x_i and take the minimum/maximum, which is analogous to a convolution layer with pooling. In practice, for efficiency concern, the memory cost of this operation is $O(T \cdot l)$. When T is large (e.g. $T > 2000$) this operation requires numerous GPU memory, mainly due to the unnecessary intermediate variables and gradients are retained . However, the traditional convolution operation does not suffer from this because of low-level optimizations from CUDA, which does not retain the intermediate gradients. Note that ShapeConv (Qu et al., 2024) makes a connection between shapelet transform and convolution by: NEW

$$d(x_i^m, s_k^{m,l}) = -2 \max_{j=1,\dots,T-l+1} \left[s_k^{m,l} * x_i^m - \frac{\|s_k^{m,l}\|_2^2 + \|x_i^m\|_2^2}{2} \right], \tag{10}$$

where $s_k^{m,l} * x_i^m$ is the convolution (cross-correlation) operation. However, we found that, in actual implementations, the additional norm term still suffers from the memory overhead.

To address this memory limitation on very long sequences, we provide two implementations for the time-memory trade-off: NEW

1. A time-efficient implementation using large matrix operations:

```
x = x.unfold(2, shapelet_length, 1)
x = x.permute((0, 2, 1, 3)).unsqueeze(2)
d = dist(x - shapelets).mean(dim=-1)
```

2. A memory-efficient implementation using loops:

```
class ShapeletDistanceFunc(torch.autograd.Function):
    def forward(ctx, x, s):
        ctx.save_for_backward(x, s)
        output = torch.cat([dist(s - x[:, :, i:i+s.shape[-1]])
            for i in range(x.shape[-1] - s.shape[-1]+1)], dim=1)
        return output
    def backward(ctx, grad_output):
        # Compute gradient of s
        return 0, grad_s

def ShapeletDistance(x, s):
    return ShapeletDistanceFunc.apply(x, s)

d = ShapeletDistance(x, shapelet)
```

On the largest datasets, this memory-efficient implementation takes less than 12 GB of GPU memory, but requires significantly more time to compute.

Another method to mitigate this issue is by using stride. For example, compared to traditional convolution operation `Conv1d()`, $s_k^{m,l}$ transforms x_i into $p_{i,k}^{m,l}$ using Equation 2 with $\texttt{in_channels} = 1$, $\texttt{out_channels} = 1$, $\texttt{kernel_size} = l$, $\texttt{stride} = 1$, $\texttt{padding} = 1$, and $\texttt{dilation} = 1$. Memory cost reduces as `stride` increase. When l is large, this would not bring significant effects since the learned shapelets are abstracted patterns. In practice, we find that setting $\texttt{stride} = \log(l)$ results in the same level of performance as $\texttt{stride} = 1$ on most datasets.

A.4 Ablation Study Setup

Ablation study in Section 5.3 is conducted on a subset of the UEA datasets which include 26 out of 30 datasets. We exclude `DuckDuckGeese`, `EigenWorms`, `MotorImagery`, and `PEMS-SF` because their dimensions lead to the issue discussed in Appendix A.3, making them inefficient to conduct large-scale hyperparameter study. For each ablation case, we only change the hyperparameter of interest and keeping other hyperparameters as the default values. A summary of the ablation results are presented in Section 5.3 and detailed results are included in Appendix B.4.

B ADDITIONAL EXPERIMENTAL RESULTS

B.1 FULL RESULTS ON 30 DATASETS FROM THE UEA ARCHIVE

Table 6: Accuracy and comparison of the methods on 30 datasets from the UEA archive. The best accuracy for each dataset is marked with bold, the second-best is marked with italic, and the third-best is marked with underline. The average and median standard deviation of InterpGN are 0.008 and 0.006.

	Classical		Deep Learning						With Interpretable Features			Ours	
Dataset	STRF	DTW	FCN	TS2Vec	TimesNet	TST	PatchTST	SVP-T	ShapeNet	RLPAM	ShapeConv	SBM	InterpGN
ArticularyWordRecognition	0.917	0.987	0.991	0.987	0.973	0.983	0.927	*0.993*	0.987	0.923	**0.994**	*0.993*	0.991
AtrialFibrillation	0.267	0.200	0.213	0.200	0.333	0.200	0.333	0.400	0.400	**0.733**	*0.521*	0.387	0.253
BasicMotions	0.925	0.975	**1.000**	0.975	0.975	0.965	0.700	**1.000**	**1.000**	**1.000**	0.997	**1.000**	**1.000**
CharacterTrajectories	0.849	0.989	*0.996*	0.995	0.987	N/A	0.976	0.990	0.980	0.978	0.981	0.982	**0.997**
Cricket	0.944	**1.000**	0.997	0.972	0.903	0.958	0.889	**1.000**	0.986	**1.000**	0.998	0.978	**1.000**
DuckDuckGeese	0.380	0.600	0.684	0.680	0.580	0.480	0.220	*0.700*	**0.725**	*0.700*	0.648	0.416	0.512
ERing	0.889	0.133	0.890	0.874	0.927	0.933	0.937	0.937	0.133	0.819	0.774	**0.966**	*0.939*
EigenWorms	0.672	0.618	0.715	0.847	N/A	N/A	N/A	**0.923**	0.878	*0.908*	0.802	0.553	0.695
Epilepsy	0.978	0.964	0.986	0.964	0.877	0.920	0.913	0.986	*0.987*	0.978	0.972	**0.993**	0.983
EthanolConcentration	**0.677**	0.323	0.293	0.308	0.285	0.337	0.259	0.331	0.312	*0.369*	0.253	0.304	0.281
FaceDetection	0.567	0.529	0.577	0.501	*0.677*	**0.681**	0.668	0.512	0.602	0.621	0.635	0.658	0.658
FingerMovements	0.500	0.530	0.634	0.480	0.530	**0.776**	0.580	0.600	0.580	*0.640*	0.587	0.600	0.620
HandMovementDirection	0.419	0.231	0.432	0.338	0.595	*0.608*	0.514	0.392	0.338	**0.635**	0.413	0.473	0.449
Handwriting	0.104	0.286	**0.615**	0.515	0.311	0.305	0.251	0.433	0.452	0.522	0.527	0.244	*0.612*
Heartbeat	0.746	0.717	0.752	0.683	0.732	0.712	0.722	**0.790**	0.756	0.779	*0.784*	0.736	0.762
InsectWingbeat	0.208	N/A	*0.654*	0.466	N/A	**0.684**	N/A	0.184	0.250	0.352	0.509	0.468	0.559
JapaneseVowels	0.676	0.949	**0.994**	0.984	0.954	**0.994**	0.935	0.978	0.984	0.935	0.993	0.963	0.989
LSST	0.491	0.551	0.415	0.537	0.382	0.381	0.519	**0.666**	0.590	*0.643*	0.608	0.633	0.601
Libras	0.817	0.870	*0.954*	0.867	0.761	0.844	0.761	0.833	0.856	0.794	0.887	0.857	**0.968**
MotorImagery	0.510	0.500	0.576	0.510	0.610	N/A	N/A	*0.650*	0.610	0.610	**0.674**	0.624	0.590
NATOPS	0.794	0.883	*0.983*	0.928	0.833	0.900	0.756	0.906	0.833	0.950	0.937	0.879	**0.984**
PEMS-SF	**0.925**	0.711	0.830	0.682	0.844	*0.919*	0.809	0.867	0.751	0.632	0.801	0.885	0.862
PenDigits	0.855	0.977	**0.989**	**0.989**	0.984	0.974	0.974	0.938	0.977	0.982	0.968	0.971	**0.989**
PhonemeSpectra	0.155	0.151	**0.326**	0.233	0.146	0.088	0.081	0.176	0.298	0.175	0.192	0.255	*0.323*
RacketSports	0.842	0.803	**0.908**	0.855	0.855	0.829	0.757	0.842	0.882	0.868	0.863	*0.897*	*0.897*
SelfRegulationSCP1	0.846	0.775	*0.915*	0.812	0.908	**0.925**	0.795	0.884	0.782	0.802	0.858	0.859	0.901
SelfRegulationSCP2	0.489	0.539	0.580	0.578	0.539	0.589	0.506	0.600	0.578	**0.632**	*0.624*	0.528	0.571
SpokenArabicDigits	0.679	0.963	*0.996*	0.988	0.988	0.993	0.977	0.986	0.975	0.621	0.979	0.994	**0.997**
StandWalkJump	0.467	0.200	0.427	0.467	0.533	0.267	0.467	0.467	0.533	**0.667**	*0.587*	0.533	0.480
UWaveGestureLibrary	0.762	0.903	0.890	0.906	0.863	0.903	0.828	*0.941*	0.906	**0.944**	0.936	0.909	0.912
Avg. Accuracy	0.645	0.650	0.740	0.704	0.710	0.709	0.669	0.730	0.697	0.740	*0.743*	0.718	**0.746**
Avg. Rank	9.633	9.000	*4.800*	7.400	7.750	6.926	9.926	5.000	6.267	5.300	5.533	5.633	**4.133**
Num. Top-1	2	1	6	1	0	5	0	5	2	**7**	2	3	**7**
Num. Top-3	2	1	**14**	2	4	8	2	13	7	**14**	10	10	12
Wins/Draws	27	27	18	26	20	18	24	18	22	18	19	20	-
Losses	3	2	12	4	8	9	3	12	8	12	11	10	-
Wilcoxon p-value	0.000	0.000	0.367	0.000	0.000	0.002	0.000	0.392	0.026	0.299	0.084	0.080	-

B.2 Additional Interpretability Analysis

B.2.1 Faithfulness

We follow Alvarez Melis & Jaakkola (2018) to asses the faithfulness of shapelets learned by the SBM. Specifically, for each concept (i.e., shapelet predicate p), we measure its relevance by calculating the change in the probability of a certain prediction before and after removing it (i.e., set $p = 0$). The faithfulness score is then determined by the correlation between the relevance of a shapelet concept and its assigned importance w. Aggregating results across all samples in the dataset, we generate the box plots shown in Figure 7. Across all five datasets, regardless of the varying performance levels of the SBM, we observe consistently high faithfulness estimates. NEW

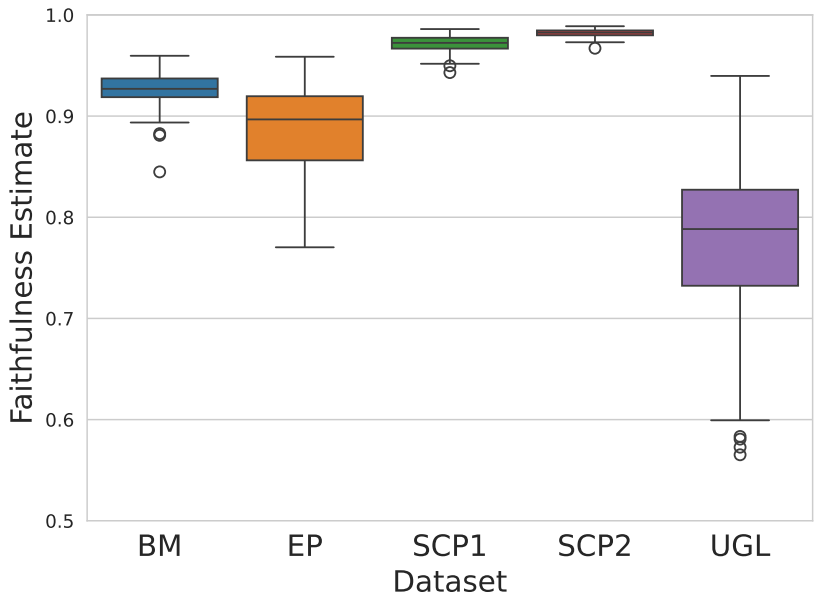

Figure 7: Faithfulness estimate: aggregated correlation statistics between shapelet concept relevance and importance.

B.2.2 VISUALIZATION OF EXPLANATIONS

Global explanations . We visualize the global explanations of the UWaveGestureLibrary, BasicMotions, SelfRegulationSCP1, and SelfRegulationSCP2 datasets. We choose these datasets since their dimensions are favored for visualizations (i.e., M and C are not too high). UWaveGestureLibrary and BasicMotions are representitives for human motion data; SelfRegulationSCP1 and SelfRegulationSCP2 are representitives for EEG data. In each figure, for each category, we visualize the time-series samples (left, in gray), the top-5 positively relevant shapelets (middle, in blue), and the top-5 negatively relevant shapelets (right, in red). NEW

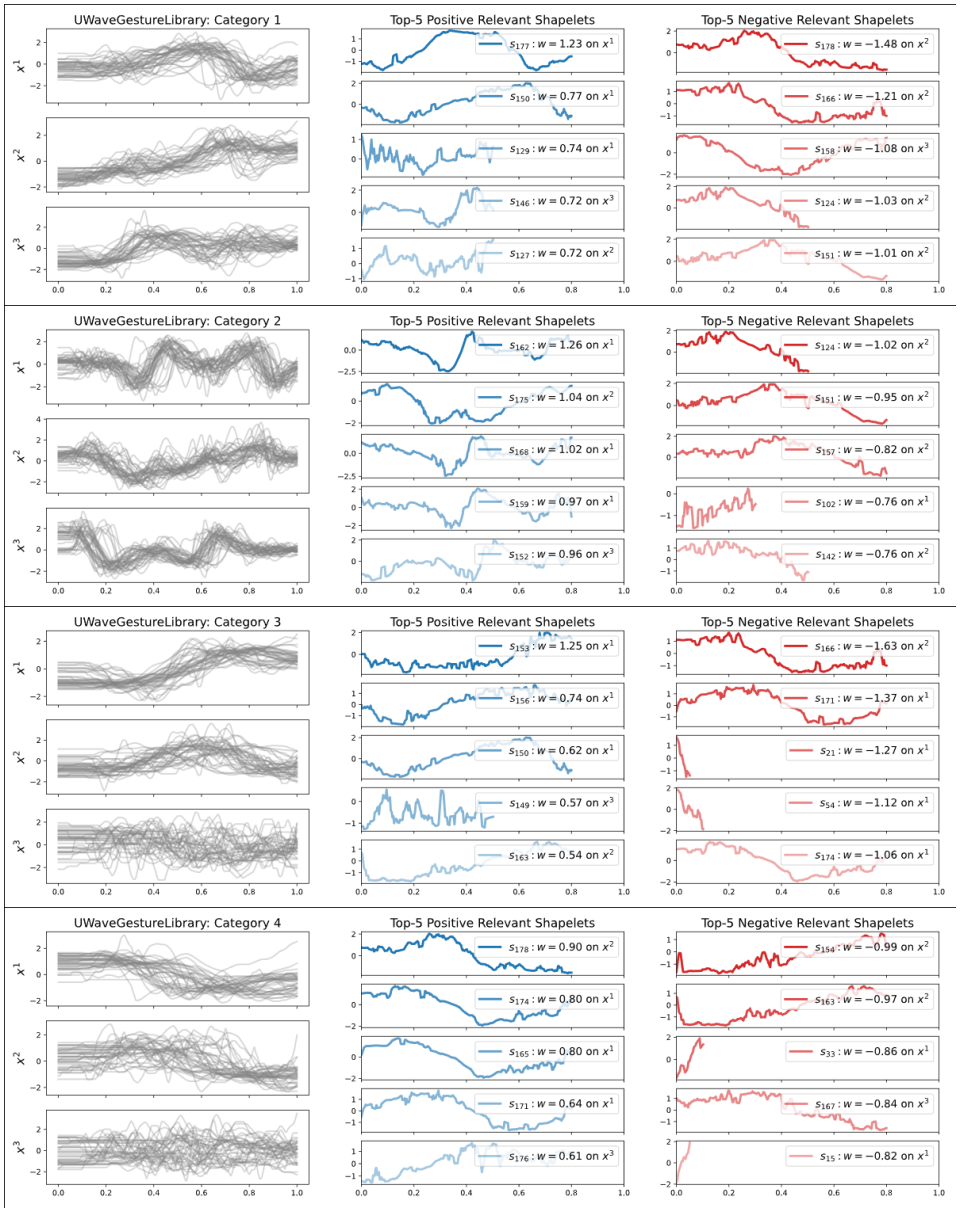

Figure 8: Global explanations of the SBM on the UWaveGestureLibrary dataset. (Part 1)

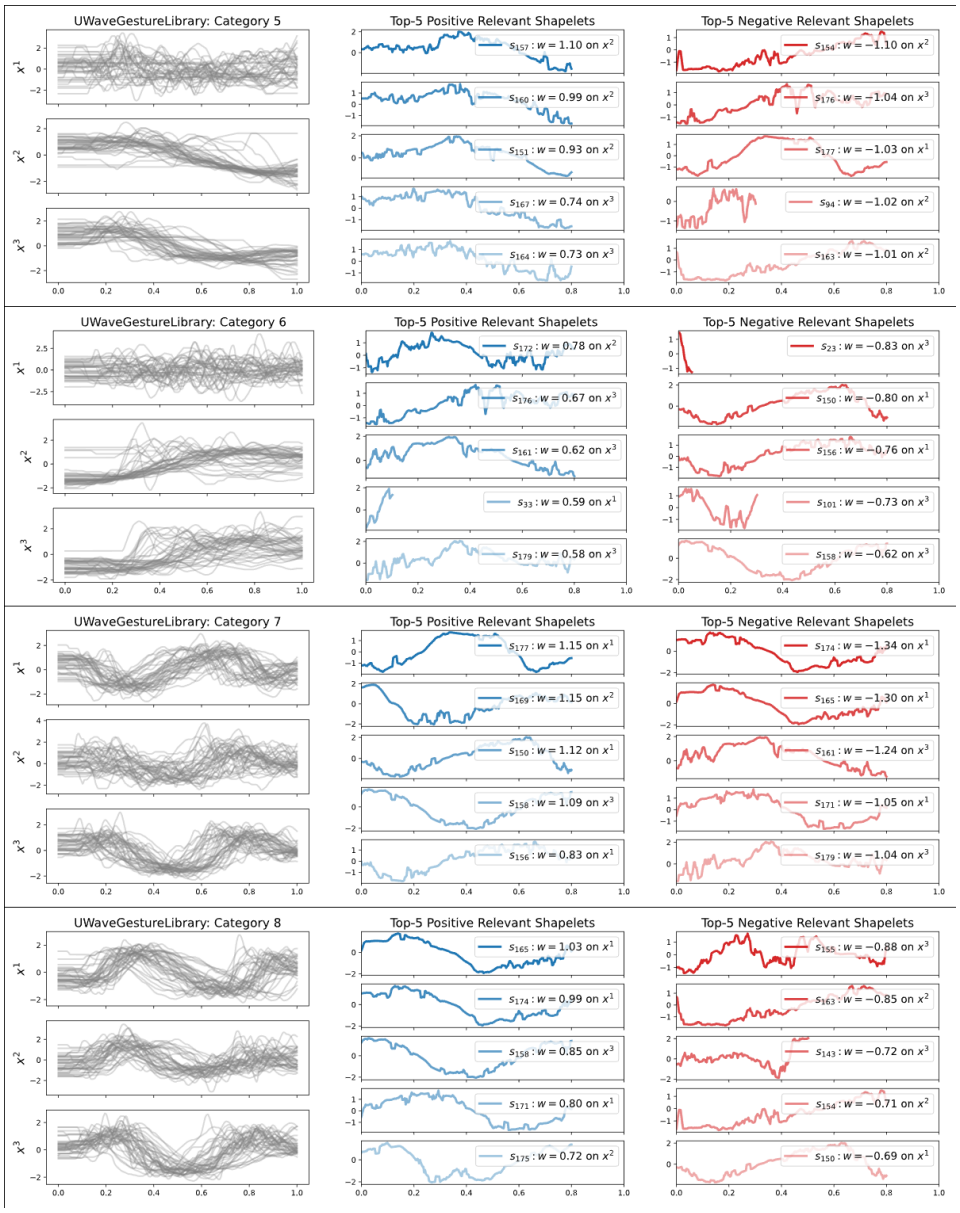

Figure 9: Global explanations of the SBM on the UWaveGestureLibrary dataset. (Part 2)

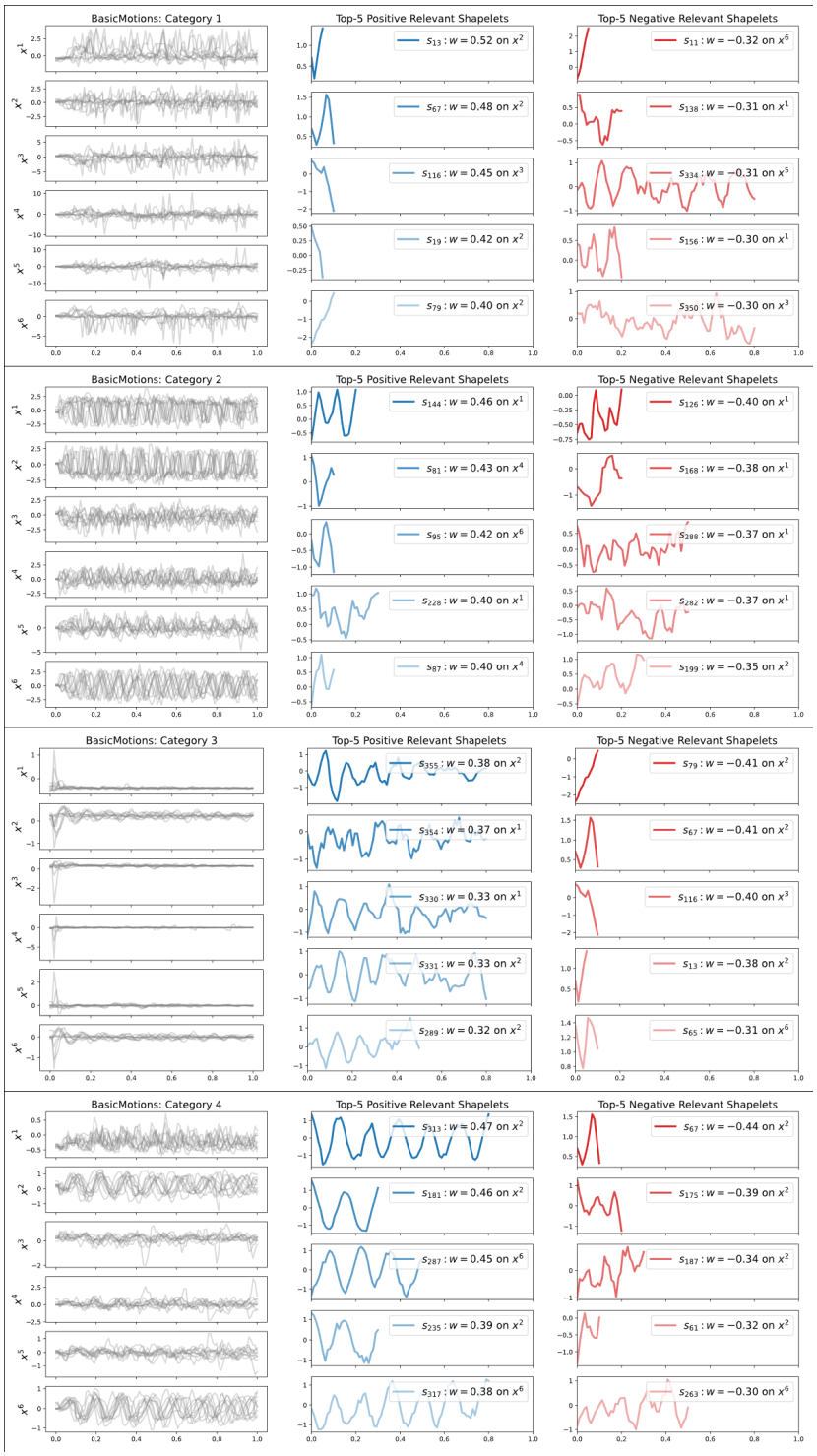

Figure 10: Global explanations of the SBM on the BasicMotions dataset.

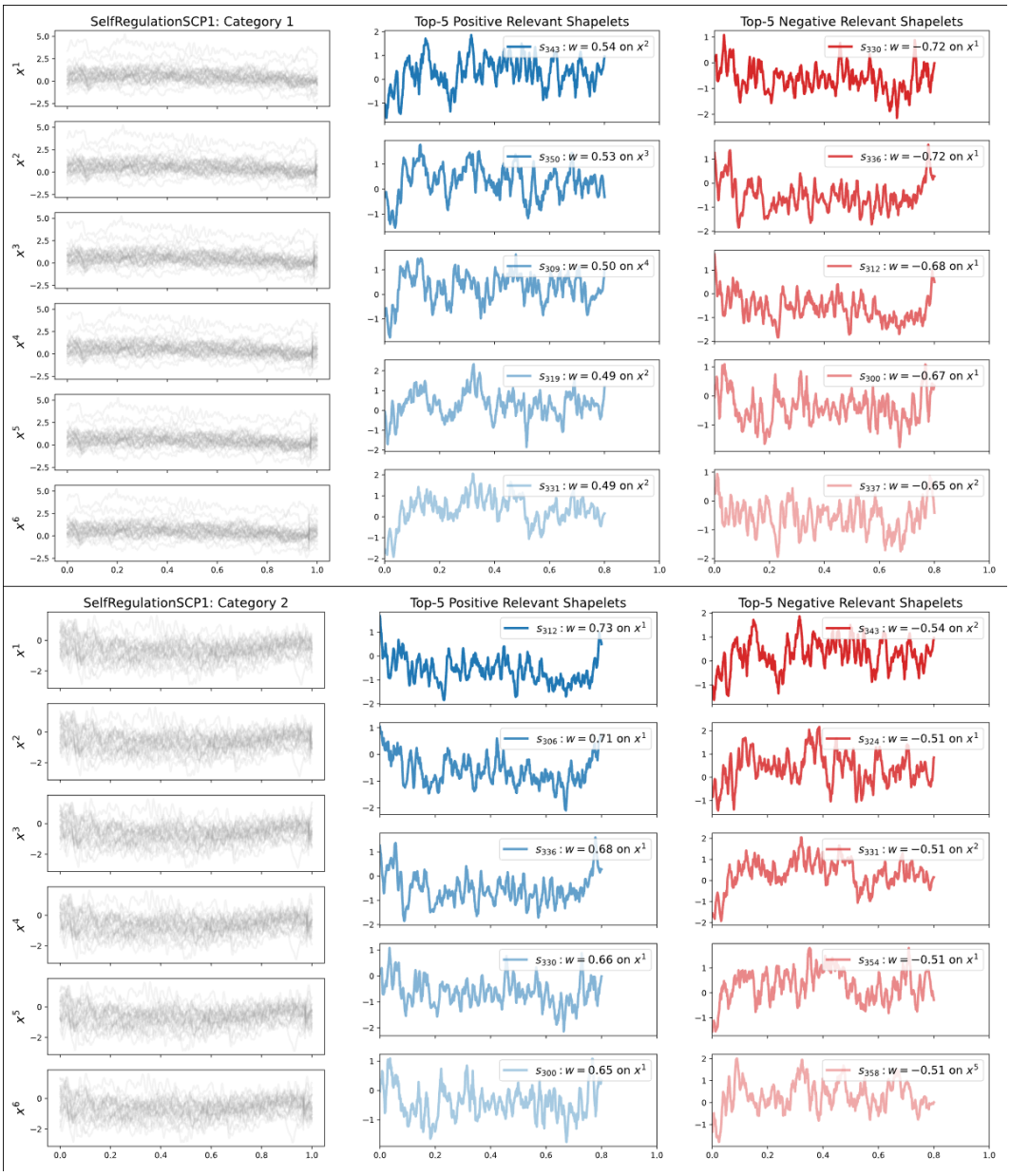

Figure 11: Global explanations of the SBM on the SelfRegulationSCP1 dataset. For clarity, we visualize 30 time-series samples.

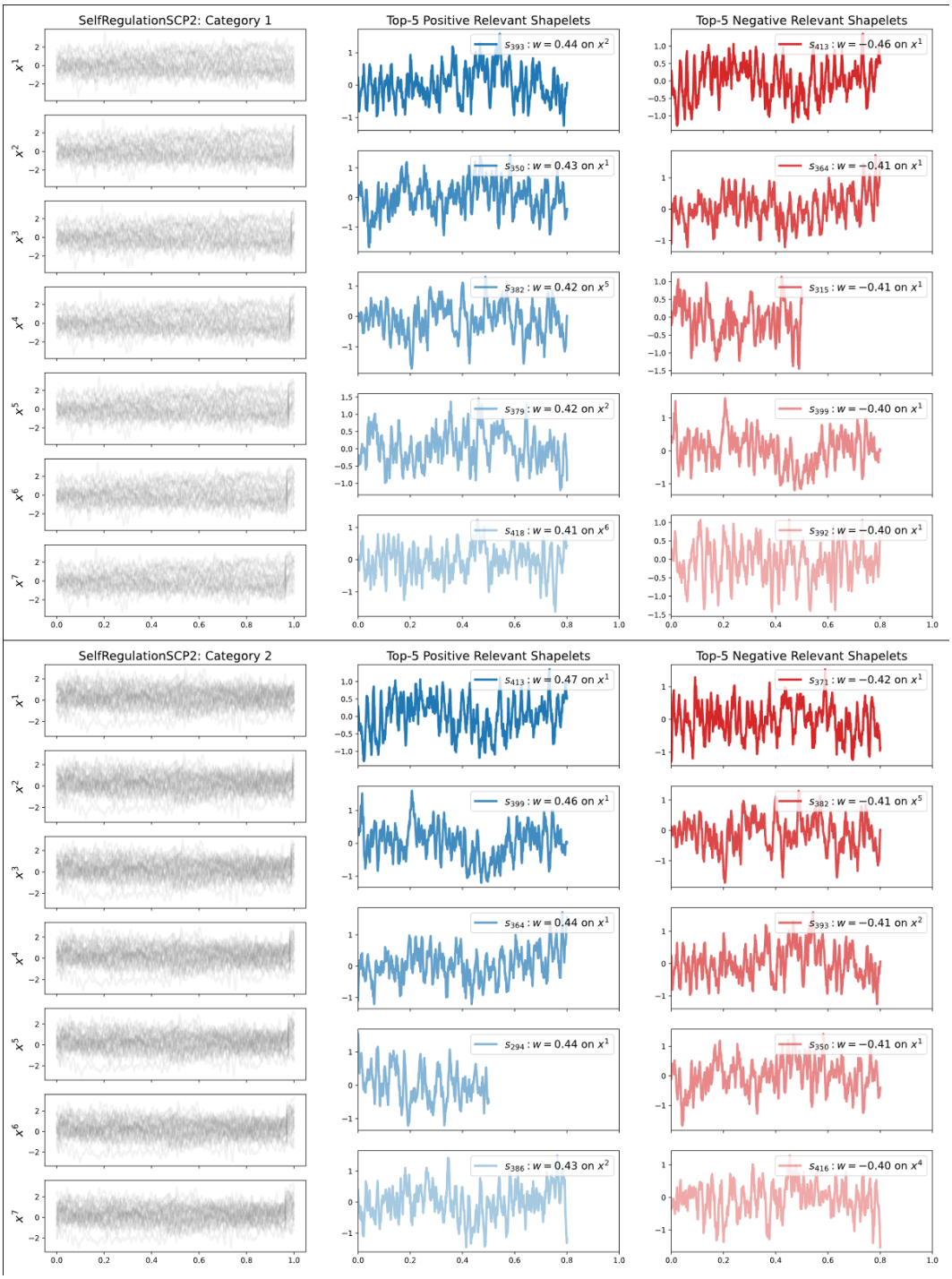

Figure 12: Global explanations of the SBM on the SelfRegulationSCP2 dataset. For clarity, we visualize 30 time-serie samples.

Local explanations. We visualize the local explanations for the four datasets. In each Figure, a sub-figure visualizes a time-series sample (in gray) along with the top-5 most important shapelets. The color of each shapelet indicates its importance, with blue representing the highest importance, followed by orange, green, red, and purple for progressively lower importance. NEW

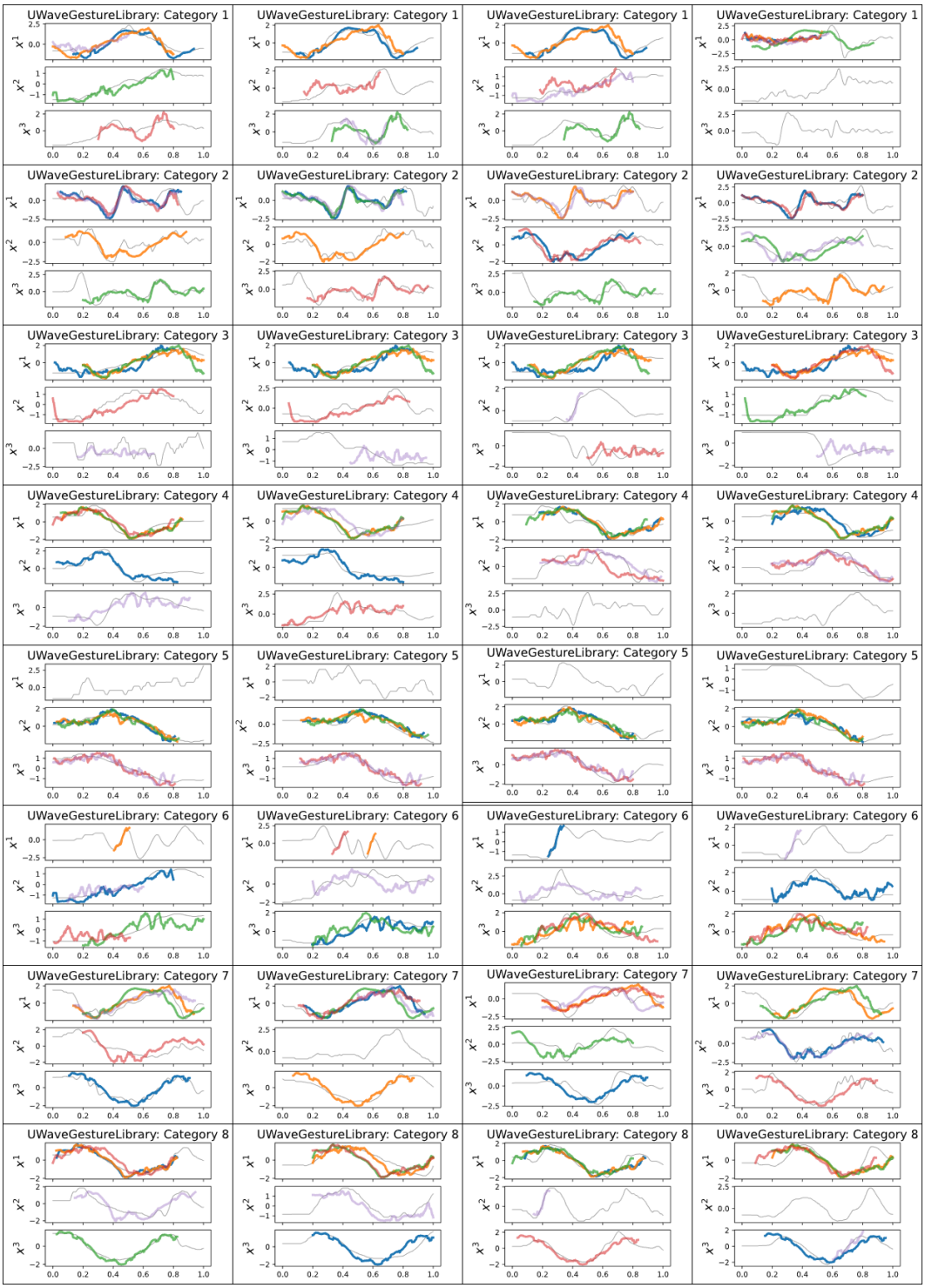

Figure 13: Local explanations of the SBM on the UWaveGestureLibrary dataset.

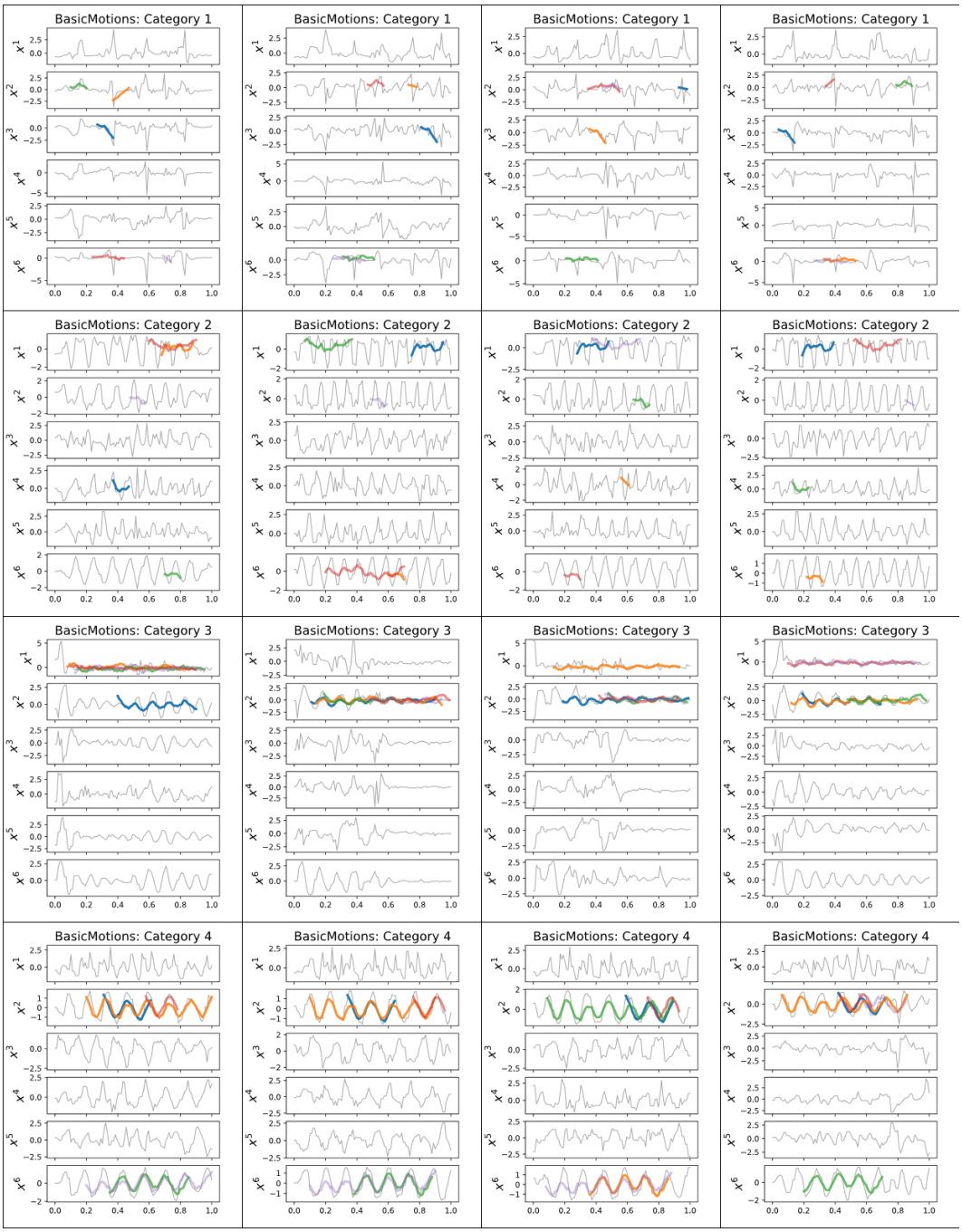

Figure 14: Local explanations of the SBM on the BasicMotions dataset.

The local explanations reflect the limitation we discussed in Section 6, where explanations for certain categories may appear counterfactual. For example, in the BasicMotions dataset, the most important shapelets for Category 1 may not represent the most characteristic features of that category. Despite this, the SBM can still make accurate predictions due to the strong feature representation for other categories. This issue becomes more pronounced in datasets with two categories, such as SelfRegulationSCP1 and SelfRegulationSCP2. These findings suggest that for binary classification tasks, using a single binary classifier with one unified "rule" might be a more effective and reasonable design, rather than assigning a separate "rule" to each class. NEW

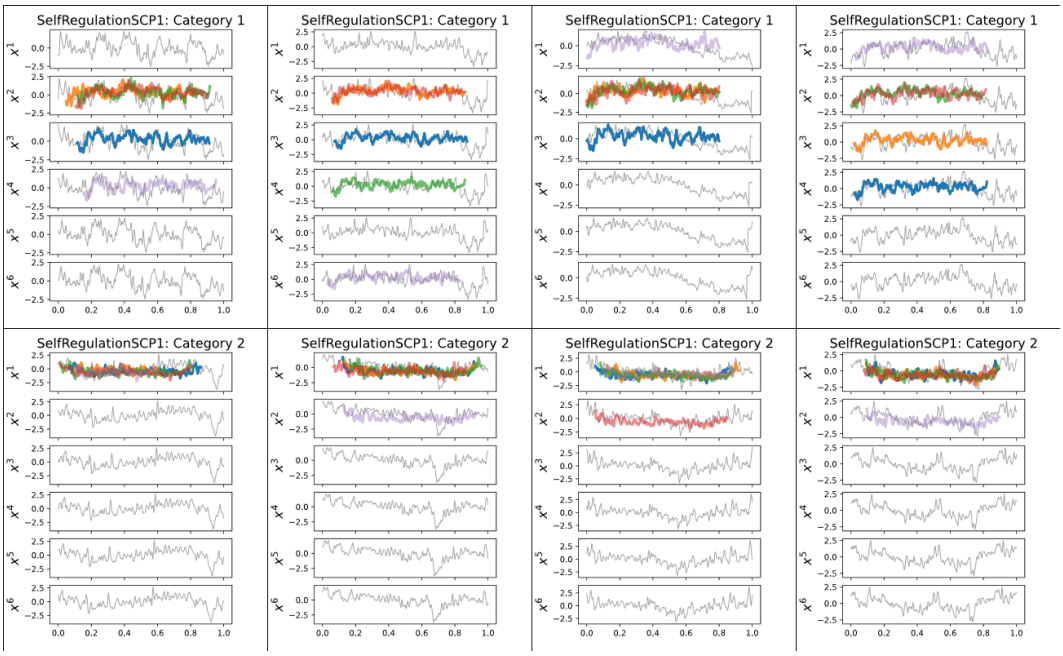

Figure 15: Local explanations of the SBM on the SelfRegulationSCP1 dataset.

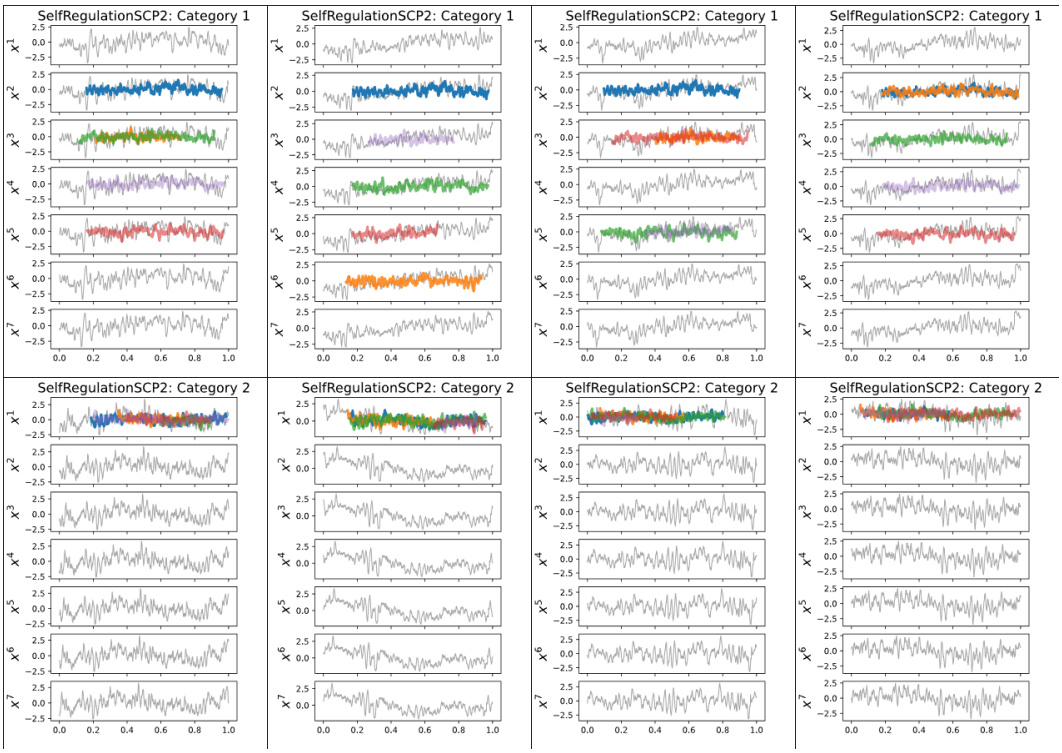

Figure 16: Local explanations of the SBM on the SelfRegulationSCP2 dataset.

B.3 BEHAVIOR OF THE INTERPRETABILITY GATING FUNCTION

In Figure 17, we present the relationship between values of $\eta(x_i)$ and predictions of InterpGN to further study the behavior of the proposed interpretability gating function. We conclude that InterpGN's predictions is consistent with SBM's predictions when $\eta(x_i)$ is high, preserving interpretability for those samples. The DNN makes corrections when $\eta(x_i)$ is low to improve performance. Note that there are cases where the DNN changes SBM's predictions to incorrect, suggesting that InterpGN's performance can be further improved using more advanced DNNs.

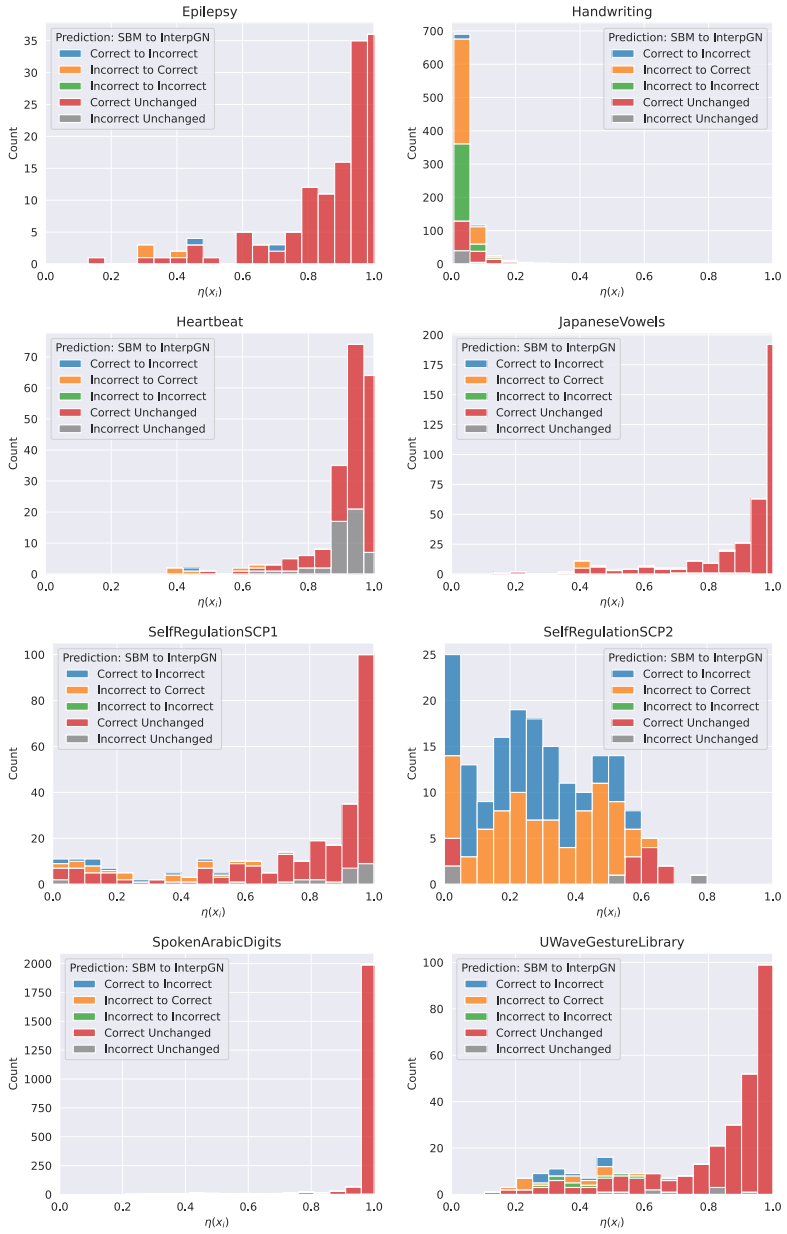

Figure 17: Histogram of values $\eta(x_i)$, and the prediction consistency between the interpretable expert and InterpGN.

B.4 Ablation Study Results

Table 7: Number of shapelet

model	K	accu.	quality	$\lvert w\rvert > 1$	$\lvert w\rvert > 0.5$	$\lvert w\rvert > 0.1$	Gini($\lvert w\rvert$)	η
SBM	5	0.725	0.129	0.057	0.179	0.644	0.454	-
SBM	10	0.733	0.098	0.032	0.097	0.531	0.461	-
InterpGN	5	0.752	0.126	0.051	0.179	0.634	0.443	0.507
InterpGN	10	0.758	0.093	0.026	0.099	0.514	0.450	0.542

Table 8: β schedule of InterpGN

β	K	accu.	quality	$\lvert w\rvert > 1$	$\lvert w\rvert > 0.5$	$\lvert w\rvert > 0.1$	Gini($\lvert w\rvert$)	η
constant	5	0.752	0.126	0.051	0.179	0.634	0.443	0.507
constant	10	0.758	0.093	0.026	0.099	0.514	0.450	0.542
cosine	5	0.751	0.108	0.039	0.123	0.574	0.457	0.445
cosine	10	0.753	0.083	0.022	0.076	0.459	0.457	0.482

Table 9: Predicate types in SBM

Predicate	K	accu.	quality	$\lvert w\rvert > 1$	$\lvert w\rvert > 0.5$	$\lvert w\rvert > 0.1$
RBF	5	0.725	0.129	0.057	0.179	0.644
RBF	10	0.733	0.098	0.032	0.097	0.531
Linear	5	0.711	0.168	0.071	0.177	0.544
Linear	10	0.722	0.119	0.048	0.117	0.446

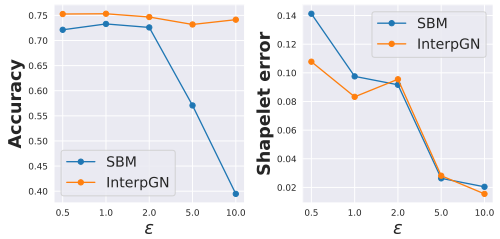

Figure 18: **Ablation on ϵ**

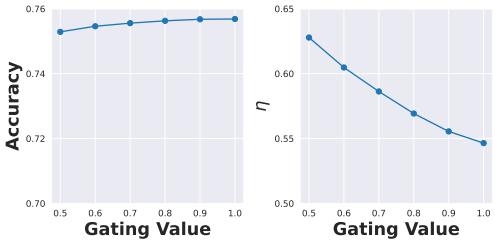

Figure 19: **Ablation on $\underline{\eta}$**

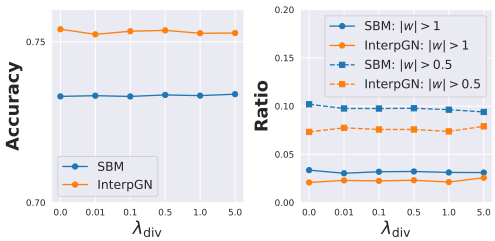

Figure 20: **Ablation on λ_{div}**

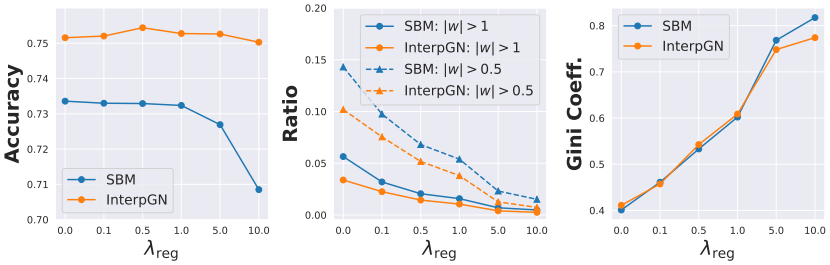

Figure 21: **Ablation on λ_{reg}**

Table 10: Full results and variations on number of shapelets K

model	K	accu.	quanlity	$\lvert w\rvert > 1$	$\lvert w\rvert > 0.5$	$\lvert w\rvert > 0.1$	η
SBM	5	0.725 ± 0.01	0.129 ± 0.02	0.057 ± 0.012	0.179 ± 0.053	0.644 ± 0.067	-
SBM	10	0.733 ± 0.007	0.098 ± 0.015	0.032 ± 0.008	0.097 ± 0.024	0.531 ± 0.054	-
InterpGN	5	0.752 ± 0.008	0.126 ± 0.02	0.051 ± 0.013	0.179 ± 0.032	0.634 ± 0.049	0.507 ± 0.047
InterpGN	10	0.758 ± 0.009	0.093 ± 0.01	0.026 ± 0.005	0.099 ± 0.017	0.514 ± 0.059	0.542 ± 0.044

Table 11: Full results and variations on β schedule in InterpGN

β schedule	K	accu.	quanlity	$\lvert w\rvert > 1$	$\lvert w\rvert > 0.5$	$\lvert w\rvert > 0.1$	η
constant	5	0.752 ± 0.008	0.126 ± 0.02	0.051 ± 0.013	0.179 ± 0.032	0.634 ± 0.049	0.507 ± 0.047
constant	10	0.758 ± 0.009	0.093 ± 0.01	0.026 ± 0.005	0.099 ± 0.017	0.514 ± 0.059	0.542 ± 0.044
cosine	5	0.751 ± 0.008	0.108 ± 0.015	0.039 ± 0.01	0.123 ± 0.027	0.574 ± 0.053	0.445 ± 0.042
cosine	10	0.753 ± 0.008	0.083 ± 0.01	0.022 ± 0.006	0.076 ± 0.014	0.459 ± 0.054	0.482 ± 0.045

Table 12: Full results and variations on ϵ

model	ϵ	accu.	quanlity	$\lvert w\rvert > 1$	$\lvert w\rvert > 0.5$	$\lvert w\rvert > 0.1$	η
SBM	0.5	0.721 ± 0.01	0.141 ± 0.018	0.034 ± 0.006	0.087 ± 0.014	0.388 ± 0.053	-
SBM	1	0.733 ± 0.007	0.098 ± 0.015	0.032 ± 0.008	0.097 ± 0.024	0.531 ± 0.054	-
SBM	2	0.726 ± 0.01	0.092 ± 0.01	0.047 ± 0.009	0.181 ± 0.043	0.619 ± 0.028	-
SBM	5	0.571 ± 0.032	0.026 ± 0.004	0.053 ± 0.007	0.099 ± 0.01	0.162 ± 0.013	-
SBM	10	0.395 ± 0.026	0.02 ± 0.003	0.041 ± 0.007	0.07 ± 0.007	0.09 ± 0.006	-
InterpGN	0.5	0.753 ± 0.009	0.108 ± 0.015	0.019 ± 0.005	0.056 ± 0.011	0.298 ± 0.046	0.292 ± 0.063
InterpGN	1	0.753 ± 0.008	0.083 ± 0.01	0.022 ± 0.006	0.076 ± 0.014	0.459 ± 0.054	0.482 ± 0.045
InterpGN	2	0.747 ± 0.01	0.096 ± 0.008	0.044 ± 0.007	0.175 ± 0.026	0.643 ± 0.033	0.635 ± 0.038
InterpGN	5	0.732 ± 0.018	0.028 ± 0.006	0.047 ± 0.008	0.093 ± 0.012	0.163 ± 0.015	0.366 ± 0.044
InterpGN	10	0.741 ± 0.011	0.015 ± 0.003	0.03 ± 0.009	0.059 ± 0.01	0.08 ± 0.011	0.148 ± 0.024

Table 13: Full results and variations on λ_{reg}

model	λ_{reg}	accu.	quanlity	$\lvert w\rvert > 1$	$\lvert w\rvert > 0.5$	$\lvert w\rvert > 0.1$	η
SBM	0	0.734 ± 0.007	0.148 ± 0.024	0.056 ± 0.009	0.143 ± 0.027	0.613 ± 0.064	-
SBM	0.1	0.733 ± 0.007	0.098 ± 0.015	0.032 ± 0.008	0.097 ± 0.024	0.531 ± 0.054	-
SBM	0.5	0.733 ± 0.007	0.074 ± 0.01	0.021 ± 0.006	0.068 ± 0.018	0.432 ± 0.048	-
SBM	1	0.732 ± 0.007	0.059 ± 0.006	0.016 ± 0.003	0.054 ± 0.012	0.343 ± 0.042	-
SBM	5	0.727 ± 0.009	0.023 ± 0.002	0.007 ± 0.001	0.023 ± 0.004	0.128 ± 0.015	-
SBM	10	0.709 ± 0.01	0.014 ± 0.001	0.005 ± 0.001	0.015 ± 0.003	0.07 ± 0.009	-
InterpGN	0	0.753 ± 0.008	0.113 ± 0.015	0.037 ± 0.007	0.105 ± 0.014	0.535 ± 0.06	0.51 ± 0.051
InterpGN	0.1	0.753 ± 0.008	0.083 ± 0.01	0.022 ± 0.006	0.076 ± 0.014	0.459 ± 0.054	0.482 ± 0.045
InterpGN	0.5	0.752 ± 0.008	0.064 ± 0.007	0.014 ± 0.004	0.051 ± 0.009	0.351 ± 0.053	0.468 ± 0.042
InterpGN	1	0.755 ± 0.008	0.051 ± 0.006	0.011 ± 0.003	0.04 ± 0.007	0.275 ± 0.04	0.447 ± 0.06
InterpGN	5	0.751 ± 0.009	0.017 ± 0.004	0.004 ± 0.001	0.012 ± 0.004	0.09 ± 0.026	0.287 ± 0.085
InterpGN	10	0.75 ± 0.011	0.009 ± 0.002	0.002 ± 0.001	0.007 ± 0.003	0.041 ± 0.016	0.208 ± 0.071

Table 14: Full results and variations on λ_{div}

model	λ_{div}	accu.	quanlity	$\lvert w\rvert > 1$	$\lvert w\rvert > 0.5$	$\lvert w\rvert > 0.1$	η
SBM	0	0.733 ± 0.007	0.096 ± 0.014	0.034 ± 0.007	0.102 ± 0.023	0.523 ± 0.063	-
SBM	0.01	0.733 ± 0.007	0.092 ± 0.012	0.03 ± 0.006	0.098 ± 0.021	0.522 ± 0.057	-
SBM	0.1	0.733 ± 0.007	0.098 ± 0.015	0.032 ± 0.008	0.097 ± 0.024	0.531 ± 0.054	-
SBM	0.5	0.733 ± 0.008	0.101 ± 0.016	0.032 ± 0.008	0.098 ± 0.024	0.525 ± 0.062	-
SBM	1	0.733 ± 0.007	0.1 ± 0.017	0.031 ± 0.01	0.096 ± 0.026	0.522 ± 0.063	-
SBM	5	0.734 ± 0.007	0.107 ± 0.015	0.031 ± 0.006	0.094 ± 0.023	0.518 ± 0.062	-
InterpGN	0	0.754 ± 0.008	0.08 ± 0.009	0.021 ± 0.004	0.073 ± 0.013	0.464 ± 0.059	0.499 ± 0.058
InterpGN	0.01	0.752 ± 0.008	0.082 ± 0.008	0.023 ± 0.004	0.077 ± 0.012	0.455 ± 0.062	0.486 ± 0.051
InterpGN	0.1	0.753 ± 0.008	0.083 ± 0.01	0.022 ± 0.006	0.076 ± 0.014	0.459 ± 0.054	0.482 ± 0.045
InterpGN	0.5	0.754 ± 0.008	0.088 ± 0.01	0.023 ± 0.005	0.076 ± 0.013	0.466 ± 0.056	0.492 ± 0.046
InterpGN	1	0.753 ± 0.008	0.088 ± 0.009	0.021 ± 0.004	0.074 ± 0.011	0.467 ± 0.059	0.501 ± 0.052
InterpGN	5	0.753 ± 0.008	0.098 ± 0.013	0.026 ± 0.008	0.079 ± 0.013	0.465 ± 0.061	0.495 ± 0.042

B.5 TRAINING CURVES

In Figure 22 and Figure 23, we visualize the loss and η during the training of InterpGN. The figures present how the loss function design $\mathcal{L}_{\text{hybrid}} = \beta\mathcal{L}_{\text{int}} + \hat{\mathcal{L}}_{\text{ce}}$ could encourage the use of SBM during training, preventing the InterpGN from collapsing into a pure DNN when possible. NEW

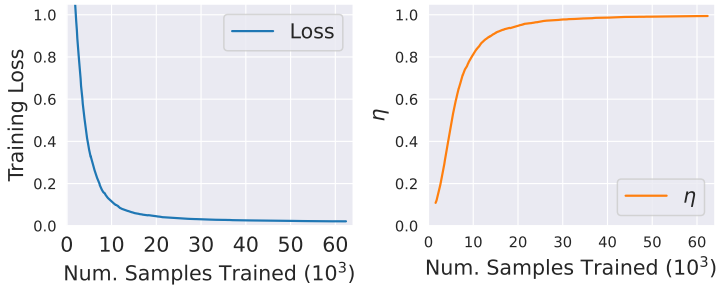

Figure 22: Training curves for InterpGN on the BasicMotions dataset: (left) L_{hybrid} and (right) average η.

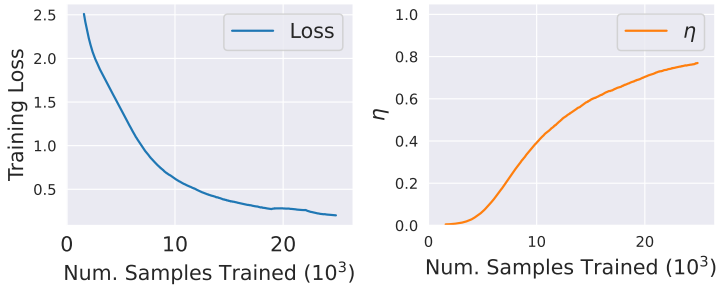

Figure 23: Training curves for InterpGN on the UWaveGestureLibrary dataset: (left) L_{hybrid} and (right) average η.

C Preliminary Results on Extended Designs

C.1 Shapelet Distance Measurements

In this paper, as defined in Equation 1, we follow the conventional definition of shapelet distance and use Euclidean distance, but the shapelet distance can be general and replaced by other metrics. Here we explore two alternative distance measures: cosine similarity and Pearson correlation. These metrics may offer favorable properties compared to Euclidean distance in some cases. For instance, cosine similarity can capture shapelets that are invariant to changes in offset. Table 15 presents the classification accuracy of SBM variants utilizing these three distance measures. The results indicate that cosine similarity and Pearson correlation can yield better performance on certain datasets, but no metric can be universally better than others. This suggests that the choice of shapelet distance metric could possibly serve as a hyperparameter requiring dataset-specific tuning depending on the needs. For example, motion datasets such as UWaveGestureLibrary may benefit from cosine similarity due to the presence of offset-invariant shapelet features. In Figure 24, we visualize an example of local explanations of SBM using euclidean distance and cosine similarity as the shapelet distance measurement, which suggests that they both could learn high-quality shapelets. NEW

Table 15: Classification accuracy of the SBM using three shapelet distance metrics. The best accuracy for each dataset is marked with bold. The training of SBM using Pearson correlation fails on the Epilepsy and UWaveGestureLibrary dataset due to infinite gradients.

Distance metric:	Euclidean	Cosine	Pearson
BasicMotions	**1.000**	0.960	0.965
Epilepsy	0.993	**0.994**	-
SelfRegulationSCP1	**0.859**	0.856	0.858
SelfRegulationSCP2	0.528	0.549	**0.557**
UWaveGestureLibrary	0.909	**0.947**	-

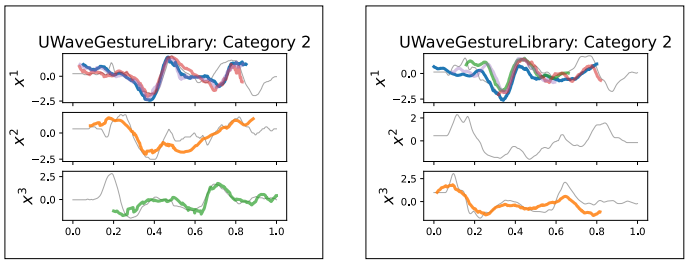

(a) SBM with Euclidean Distance (b) SBM with Cosine Similarity

Figure 24: Local explanations of SBM using (a) euclidean distance and (b) cosine similarity as the shapelet distance measurement.

C.2 Classifier Architecture in SBM

In this paper, we focus on using a linear classifier with shapelet predicates, in line with existing shapelet-based methods. While the linear classifier is often preferred for its interpretability, its simplicity introduces limitations such as neglect of the interaction/correlation among shapelets, as discussed in Section 6. To mitigate the issues, we present two additional classifier architectures: a bi-linear classifier and an attention-based classifier. Here, for simplicity, we denote the set of shapelets predicates as $\mathbf{p}_i = [p_{i,1}, \ldots, p_{i,|\mathcal{S}|}]$. Specifically, they are formulated as NEW

- Bi-linear classifier:

$$r_{i,c} = \sum_{k=1}^{|\mathcal{S}|} w_k \, p_{i,k} + \sum_{k=1}^{|\mathcal{S}|} \sum_{j=1}^{|\mathcal{S}|} \mathbb{1}(k \neq j) w_{j,k} \, p_{i,k} \, p_{i,j}. \tag{11}$$

- Attention-based classifier:

$$r_{i,c} = \sum_{k=1}^{|\mathcal{S}|} w_k \cdot \texttt{attention}(Q(\mathbf{p}_i) + \texttt{PE}, K(\mathbf{p}_i) + \texttt{PE}, p_{i,k}), \tag{12}$$

  where `attention` is the scaled dot-product attention, `PE` denotes the positional embeddings, Q and K are learnable linear projections. In our implementations, we keep low-dimensional projections $Q : \mathbb{R}^1 \mapsto \mathbb{R}^{16}$ and $K : \mathbb{R}^1 \mapsto \mathbb{R}^{16}$.

Compared to the linear classifier, the bi-linear and attention-based classifiers can capture relationships between shapelet concepts while retaining some level of interpretability. For example, the bi-linear classifier could express "shapelet s_k and s_j both exist in x_i". Although the attention mechanism (i.e., Q and K projections) may not be considered as fully interpretable, $\texttt{attention}(Q(\mathbf{p}_i) + \texttt{PE}, K(\mathbf{p}_i) + \texttt{PE}, p_{i,k})$ produces predicates that combines shapelet predicates based on attention weights, which preserves some level of interpretability

In Table 16 we compare the three SBM classifier architectures on a subset of the UEA datasets. Our results indicate that the advanced classifiers improve performance for both SBM and InterpGN on certain datasets. Interestingly, the bi-linear classifier learns shapelets of higher quality compared to the other two classifiers. Considering the simplicity, good interpretability of linear classifier and its comparable performance to more advanced classifiers on most datasets, we suggest that it is still favorable to use linear classifier in practice; however it is good to try more advanced classifiers to achieve better performance. We will also leave the exploration of other advanced classifiers (such as energy-based or graph-based ones) for future work. NEW

Table 16: Classification accuracy and shapelet quality for the three SBM classifier architectures. The best accuracy for each dataset and model is marked with bold. The best shapelet quality for each dataset and model is marked with underline.

Model:	SBM						InterpGN					
Classifier:	Linear		Bi-linear		Attention		Linear		Bi-linear		Attention	
Metric:	accu.	quality	accu.	quality	accu.	quality	accu.	quality	accu.	quality	accu.	quality
BasicMotions	**1.000**	0.044	**1.000**	0.014	**1.000**	0.037	**1.000**	0.039	**1.000**	0.018	**1.000**	0.036
Epilepsy	0.993	0.108	**1.000**	0.014	0.974	0.094	0.983	0.082	**1.000**	0.022	0.988	0.097
SelfRegulationSCP1	**0.859**	0.079	**0.859**	0.019	0.835	0.047	**0.913**	0.057	0.882	0.019	0.891	0.056
SelfRegulationSCP2	0.528	0.093	0.536	0.019	**0.573**	0.084	0.571	0.063	0.544	0.017	**0.583**	0.049
UWaveGestureLibrary	**0.909**	0.093	0.902	0.026	0.848	0.083	0.912	0.071	**0.916**	0.031	0.911	0.070